Characterization of the novel human protein methyltransferase METTL20

Helge-André Dahl

Thesis for the Masters' degree in Molecular Bioscience
Main field of study in Molecular Biology

60 study points

Department of Biosciences
Faculty of mathematics and natural sciences

UNIVERSITY OF OSLO

06/2014

2014

Characterization of the novel human protein methyltransferase METTL20

http://www.duo.uio.no/

Print: Reprosentralen, Universitetet i Oslo

Acknowledgement

The work presented in this thesis conducted in the Pål Falnes group at the Department of Biosciences of the University of Oslo between August of 2013 and June of 2014.

I would like to thank professor Pål Falnes for allowing me to work on this project as part of his group. The seemingly endless knowledge combined with his door always being open have greatly aided me with my progress as well as making me feel welcome and comfortable during my stay.

I would also like to give my co-supervisor Dr. Jedrzej Malecki special thanks. His vast experience and knowledge have ensured that I received the greatest advice ensuring a high success rate for my experiments. I am also grateful for his patience with me, and always being available to aid me with my work.

Thank you to the rest of the group for making the days fun and lively, as well as helping me with both small and big questions. It has been a joy working among you all, not only to learn from you, but also for the social aspects such as our trips out.

I am also grateful for the help from Anders Moen for his work with mass spectrometry (MS) for us, despite not working directly with you. Without the MS data that I received via Dr. Malecki, I would not have been able to complete this project.

In the same manner as I thank Mr. Moen, I thank the ABI lab for performing sequencing of my samples, allowing me to continue with my work knowing that I had the correct plasmid constructs.

A deep gratitude goes out to Shelley, for making my life outside of work and education a blessing along with our furry child Link. The deep gratitude extends to the remainder of my family, for believing in my success and constant support. Without these people in my life, I would not be who or where I am today.

Oslo, May 2014

Helge-André Dahl

Abstract

Protein methylation is a post-translational modification best studied in regards to histones and the histone code. In recent years, more studies have begun to unearth non-histone protein methylation, in most cases however, the responsible enzymes remain unidentified. Methylation of non-histone proteins could impart new characteristics, such as altering protein-protein interactions, stability, localization, and/or enzymatic activities. Recently, a novel family of ten lysine specific methyltransferases (KMTs) was identified, of which only a few have thus far been characterized. These include valosine-containing protein KMT (VCP-KMT) (Kernstock et al., 2012), calmodulin-KMT (Magnani et al., 2010) and heat shock protein 70-KMT (Hsp70-KMT)(Jakobsson et al., 2013). Characterization of the remaining members of this family, including methyltransferase like 20 (METTL20), would expand the knowledge of non-histone methyltransferases. In this study, data are presented that reveal the identity of two proteins in *Agrobacterium tumefaciens* (*A. tumefaciens*) that are substrates of the bacterial orthologue of METTL20. The sites of methylation for each substrate were ascertained by mutagenesis and fluorography. To elucidate the biological role of the bacterial orthologue of METTL20, a strain of *A. tumefaciens* was generated with a knockout (KO) of the METTL20 gene. Wild type (WT) and KO bacteria were subject to various growth conditions and stresses in an attempt to uncover a condition in which one strain outperformed the other in regards to viability and/or growth. A potential phenotype was discovered that could involve the viability and ability to grow under certain stress conditions.

Abbreviations

MTase	Methyltransferase
7BS	Seven beta strand
METTL20	Methyltransferase like 20
RpL7/L12	Ribosomal protein L7/L12
mRpL12	Mitochondrial ribosomal protein L12
ETF	Electron transfer flavoprotein
ETFα, ETFβ	ETF alpha subunit, ETF beta subunit
ETFβ1	Electron transfer flavoprotein beta subunit isoform 1
A.tumefaciens	*Agrobacterium tumefaciens*
H.sapiens	*Homo sapiens*
E.coli	*Escherichia coli*
WT / KO	Wild-type / Knockout
SAM / SAH	S-adenosyl-methionine / S-adenosyl-homocysteine
rRNA, tRNA, mRNA	Ribosomal RNA, transfer RNA, messenger RNA
EF-Tu, EF-G	Elongation factor thermal unstable, elongation factor G
IF2	Initiation factor 2
GTPase	Guanosine triphosphate hydrolase
SET	**S**uppressor of variegation 3-9, **E**nhancer of zeste and **T**rithorax
DNA, RNA	Deoxyribonucleic acid, ribonucleic acid
FAD(H/H_2)	Flavin adenosine dinucleotide (semiquinone/fully reduced)
AMP/ADP/ATP	Adenosine mono-, di- and tri-phosphate
ETF:QO	ETF ubiquinone oxidoreductase
NAD(H)	Nicotinamide adenine dinucleotide (reduced)
MCAD	Medium chain fatty-acid dehydrogenase
IVD	Isovaleryl-CoA dehydrogenase
GCD	Glutaryl-CoA dehydrogenase
SARD	Sarcosine dehydrogenase
DMGD	Di-methylglycine dehydrogenase
THF	Tetrahydrofolate
IEP	Intron-encoded protein
IBS	Intron binding site
EBS	Exon binding site
RNP	Ribonucleoprotein
Tet	Tetracycline
Km	Kanamycin
IPTG	Isopropyl β-D-1-thiogalactopyranoside
MS	Mass spectrometry
Rif	Rifampicin
Gent	Gentamycin

Table of Contents

1. Introduction

1.1 Biological methylation

Methylation is a modification where a methyl group is transferred from a donor molecule to a recipient molecule. The recipient molecules are diverse and differ in both size and biophysical properties, including deoxyribonucleic acid (DNA), ribonucleic acid (RNA), metabolites, fatty acids or proteins [reviewed in(Schubert et al., 2003)]. The methylation reactions are catalyzed by methyltransferases (MTases). The most widely used donor molecule is S-adenosyl-methionine (SAM), which consists of adenosine with a bound methionine group. The transferal of the methyl group to the substrate proceeds by a S_N2 reaction in which the nucleophile group of the substrate attacks the electrophile methyl group of SAM (figure 1.1). The bi-product of methylation is S-adenosyl-homocysteine (SAH). In cells, SAH is broken down by adenosylhomocysteinase to homocysteine (and adenosine). Homocysteine is either degraded or used in the methionine cycle in which SAM is regenerated (Finkelstein, 1998). Other methyl donors include methanol, methyl tetrahydrofolate, mono-, di-, and trimethylamine, methanethiol, methyl tetrahydromethanopterin, and chloromethane. These donors generally function in reactions together with the cofactor vitamin B12 (Ragsdale, 2008).

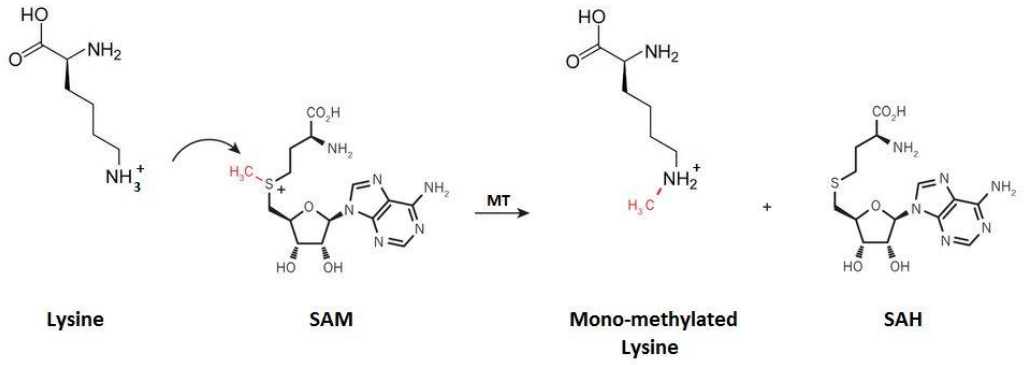

Figure 1.1 General S_N2 reaction mechanism of SAM-dependent methyltransferases. *The nucleophile amino group of Lysine, the substrate in this example, attacks the electrophile methyl group located on the methionine group of SAM. The electrophile nature of the methyl group is made possible due to the sharing of electrons by the sulphur atom, generating a positive charge (resembles a sulfonium ion). The bond between sulphur and the methyl group is thereby weakened, allowing the transfer of the methyl group. The end-products are a mono-methylated Lysine and SAH.*

1.1.1 Protein methyltransferases

Methylation of proteins occurs on several amino acid residues, including Lysine and Arginine amongst others (Clarke, 2013; Patananan et al., 2013). Lysine and Arginine are the most common residues targeted for methylation, adding methyl groups to their amino groups. Arginine residues can be mono- and di-methylated, and due to the presence of two potential methylation sites, the methylation may occur in a symmetric or asymmetric fashion (figure 1.2a). Lysine contains a single amino group in its side-chain, which can be mono-, di- and tri-methylated (figure 1.2b). Although the amino group is polar and hydrophilic, the length and nature of the side-chain renders Lysine hydrophobic. For this reason, lysine residues generally only expose the terminal amino "head" to the solvent. The purpose of post-translational modifications (PTMs) are to expand the proteome beyond that which is encoded for in the

genome, by allowing alterations of the standard 20 amino acid residues and changing their biophysical properties such as size or polarity.

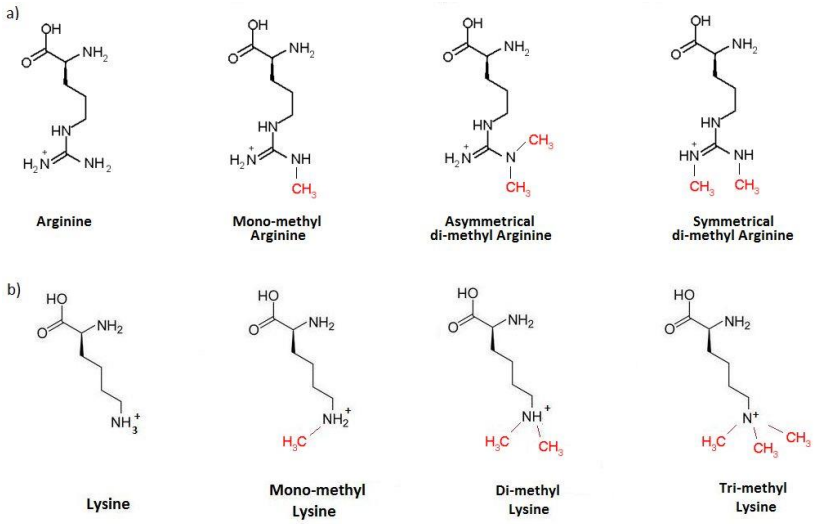

Figure 1.2 Methylation states of lysine and arginine *The possible methylation states of a) Lysine including mono-, di- and tri-methylation and b) Arginine including mono- and di-methylation, the latter in either an asymmetric or symmetric fashion.*

1.1.2 METTL20 as member of seven beta strand methyltransferases

Seven beta strand methyltransferases (7BS) is the largest of the three SAM dependent structural groups of MTases, followed by SET domain and finally membrane-bound methyltansferases. SET domain is named after three histone KMTases (**S**uppressor of variegation 3-9, **E**nhancer of zeste and **T**rithorax) from *Drosophila melanogaster*, containing a common conserved region. A common feature to the 7BS MTases is the "SAM dependent MTase fold" which has seven β-strands at the core with strand 7 antiparallel to the others and placed between strands 5 and 6. The β-strands and α-helices of the core alternate until β-strand 6, which is linked to β-strand 7 by a coil (figure 1.3). Outside this common core structure lies other protein domains involved in substrate specificity and potentially other functions.

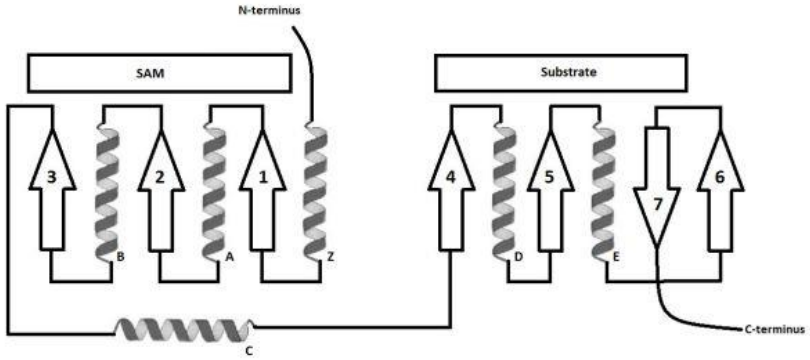

Figure 1.3 The 7BS core structure *Common structure with SAM and substrate binding sites depicted according to Martin and McMillan, 2002. Beta strands depicted as arrows, and alpha helices as gray helical ribbons.*

METTL20 belongs to Family 16 (Fam16) of the 7BS MTases, as it contains the conserved motifs belonging to 7BS MTases as well as the added (D/E)XX(Y/F) motif specific for Fam16 (figure1.4)(Kernstock et al., 2012).

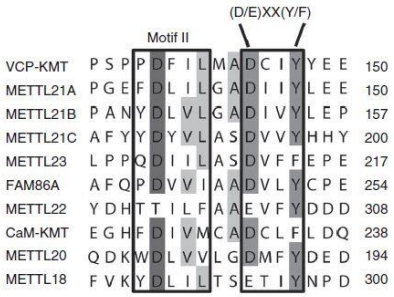

Figure 1.4 Alignment of Fam16 MTases. *Alignment with focus on the region including motif II which is one of the motifs common to all 7BS MTases, and including the (D/E)XX(Y/F) motif, common to the Fam16 MTases. Figure taken directly from (Kernstock et al., 2012), Figure 6a.*

The motifs specific for 7BS MTases in general are motifs I, post I, II and III, shown over the METTL20 protein sequence alignment of *H. sapiens* and *A. tumefaciens* (figure 1.5a). These four 7BS common motifs, together with some additional proximal residues, are involved in the binding of SAM and the substrate. They are also involved in shaping the structure involved in positioning of SAM and the substrate correctly relative to one another, in order to allow for the methylation. The sequence of motifs are used together with the spacing between them in increasingly sensitive algorithms for identification of novel 7BS MTases (Petrossian and Clarke, 2009).

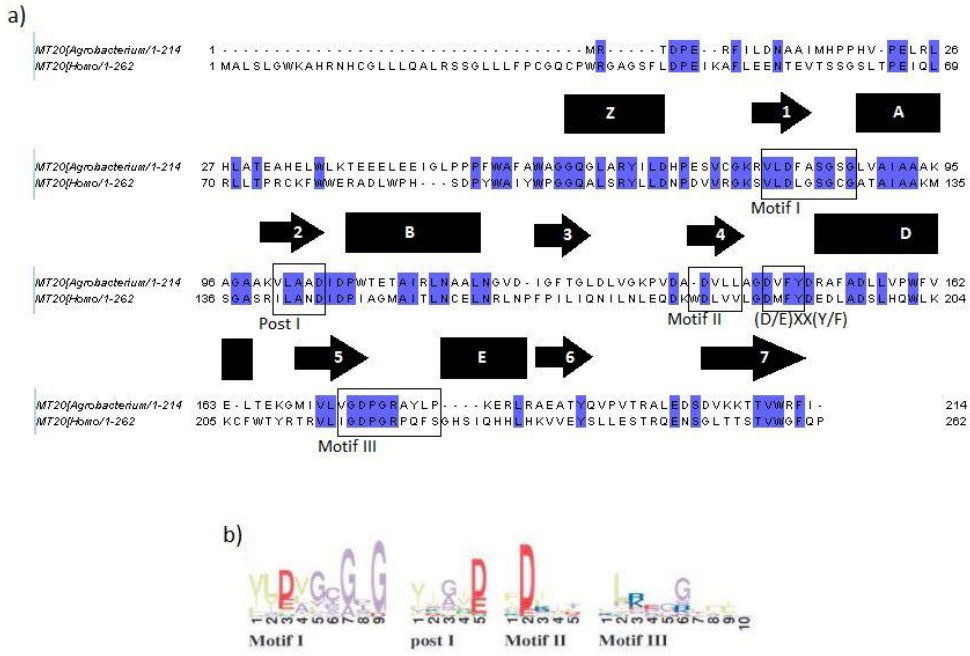

Figure 1.5 METTL20 7BS common structure and motifs*. a) METTL20 sequence alignment of A.tumefaciens (RefSeq:AAK88369.1) and H.sapiens (RefSeq:NP_001129335.1) performed using MUSCLE (Edgar, 2004), with the common 7BS core structures indicated (beta strands as filled black arrows and alpha helices as filled black boxes). The structures were predicted using YASPIN (Lin et al., 2005). The common 7BS motifs are boxed and labelled, using the b) characteristic motifs (Katz et al., 2003), and including the (D/E)XX(Y/F) motif common to Fam16 (Kernstock et al., 2012).*

The localization of METTL20 had been indicated as being pre-dominantly localized to cytoplasmic granular foci (Cloutier et al., 2013). A separate study indicates that METTL20 is not localized in cytoplasmic granular foci, but rather that it is a mitochondrial enzyme (Malecki et al., unpublished).

1.2 Ribosomal proteins

The ribosomal proteins, together with ribosomal RNA (rRNA), forms the ribonucleoparticles more commonly known as the ribosomes. Ribosomes are responsible for the translational process in which messenger RNA (mRNA) sequences are converted to the peptide sequences they encode. The ribosome is comprised of two main structures (subunits), of which the smaller subunit binds the mRNA and is responsible for the accurate matching of the transfer RNAs (tRNAs) and the nucleotide sequence. The larger subunit binds the tRNA and amino acids, and is responsible for the peptide bond formation. Eukaryotic and prokaryotic ribosomes differ in size and composition, however their function and basic design are very similar (Alberts et al., 2007). The function of individual proteins has been difficult to ascertain, as there is a large number of proteins all of which interact and cooperate with each other and the rRNA. Although the main functions of ribosomal proteins lie within protein synthesis, there is evidence that they may also carry extra-ribosomal functions. Examples of these functions include a form of self-regulation of rRNA and ribosomal protein synthesis, and stimulation of p53 expression in damaged cells (Warner and McIntosh, 2009).

1.2.1 Ribosomal protein L7/L12

Ribosomal protein L7/L12 (RpL7/L12) is the *A.* tumefaciens homologue of *H.* sapiens mitochondrial ribosomal protein L12 (mRpL12). The RpL7 and RpL12 proteins are identical, except for an N-terminal acetylation in RpL7 that is not present in RpL12. RpL7/L12 is the only of the ribosomal proteins to appear in more than one copy per ribosome, in total four copies are present on the *E. coli* ribosome. It binds the 23S rRNA of the large subunit via RpL10 (RpL10), by forming a pentameric structure (RpL10 $(RpL7/L12)_4$) which binds as one or two dimers. The RpL10 $(RpL7/L12)_4$ dimers bind adjacent to the RpL11 binding site, and form the flexible stalk of the 50S large subunit. The ribosomal stalk is involved in the binding of translational factors, including elongation factor thermal unstable (EF-Tu), elongation factor G (EF-G) and initiation factor 2 (IF2). The stalks flexibility allows the C-terminal region of RpL7/L12 to move about increasing the chances of it to come in contact with translational factors and promote its binding to the ribosome (Kothe et al., 2004). The main function of RpL7/L12 towards the elongation factors appears to be related to guanosine triphosphate hydrolase (GTPase) activation, potentially by inducing the catalytically active conformation of the GTPase domain (Mohr et al., 2002; Stelzl et al., 2001). In the case of IF2, the primary role appears to be recruitment, as the rates of subsequent steps following recruitment to the pre-initiation complex were unaffected in the absence of RpL7/L12 in regards to IF2 function (Huang et al., 2010). Mutations of RpL7/L12 performed by Diaconu et al. did not significantly reduce the overall binding efficiency of the elongation factors, however the accuracy of translation decreased significantly. This is mainly due to the elongation factors' role in translational accuracy, as the GTPase activity is induced when the correct tRNA matches

correctly to the mRNA (Diaconu et al., 2005). Figure 1.6 shows the ribosomal stalk, including a structure of RpL7/L12 interacting with EF-G.

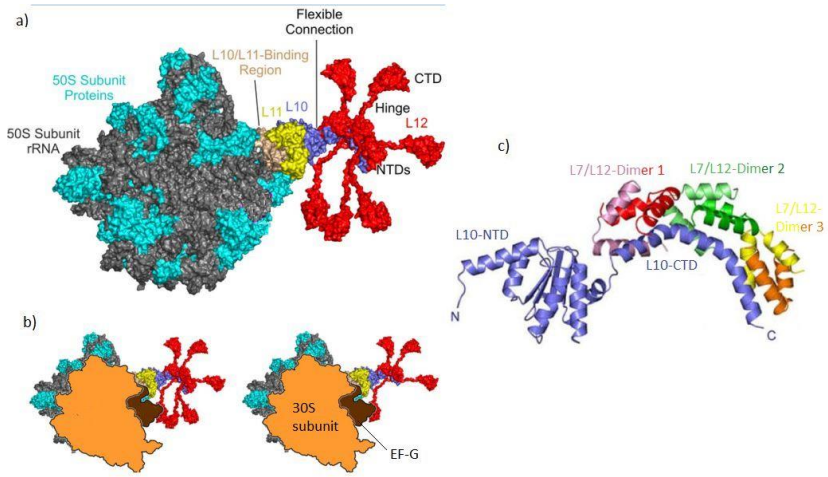

Figure 1.6 Structure of the ribosomal stalk*. a) Multiple RpL7/12 (red) dimers bound to the c-terminal region of RpL10 (blue). The c-terminal domains of the RpL7/L12 are shown in theoretical positions to illustrate their range of motion. b) Image of RpL7/L12 in the presence of EF-G bound to the ribosome and c) the dimerization of the N-terminal RpL7/L12 domains to the C-terminal RpL10 domain. Adapted from (Diaconu et al., 2005).*

1.3 Electron transfer flavoprotein

Electron transfer flavoprotein (ETF) is a heterodimer comprised of an alpha (α) and beta (β) subunit, with one flavin adenine di-nucleotide (FAD) molecule and one adenosine mono-phosphate (AMP) molecule per dimer as co-factors. The ETF is responsible for the transfer of electrons from at least nine dehydrogenases to the electron transport chain in mammals. Five such dehydrogenases are described in section 1.3.2. ETF transfers electrons from primary dehydrogenases to the membrane-bound ETF ubiquinone oxidoreductase (ETF:QO) which oxidize the FAD co-factor of ETF and brings the electrons into the electron transport chain's quinone pool. This is another entry point for electrons into the electron transport chain in addition to electrons donated by reduced nicotinamide adenine dinucleotide (NADH) primarily produced in the citric acid cycle (Simkovic and Frerman, 2004). The structure of ETF encompasses three domains, domains I to III. Domain I is mainly comprised of ETFα while domain III is comprised solely of ETFβ. These two domains form a rigid structure on which domain II rests, the domain that interacts with the FAD co-factor. Domain III contains a buried AMP molecule, which is proposed to play solely a structural role (figure 1.7)(Toogood et al., 2007).

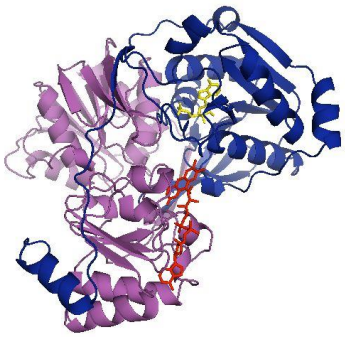

Figure 1.7 Structure of ETF. *The alpha subunit shown in magenta, the beta subunit in blue. The AMP molecule shown as yellow stick figures, buried in a cleft of the beta subunit. The FAD molecule shown as red stick figures, interacting mainly with the alpha subunit. Visualization was performed using PyMol (PDB: 1EFV)(Schrodinger, 2010).*

1.3.1 Flavin adenine dinucleotide

FAD is a redox co-factor that is involved in metabolic processes, capable of both reduction and oxidation. FAD is comprised of two main structures, a riboflavin moiety that is comprised of a ribitol and flavin, and a molecule of adenosine di-phosphate (ADP). The riboflavin is bound to ADP through its phosphate group (figure 1.8a). Dehydrogenases that either have a FAD co-enzyme or have FAD covalently bound, are capable of performing the redox reaction in which a substrate is oxidized while the FAD is reduced to its semiquinone state (FADH) or fully reduced to $FADH_2$ (figure 1.8b). When fully reduced to $FADH_2$, the aromatic ring is lost, and the energy needed to hold its conformation increases, deeming $FADH_2$ a carrier of high-energy electrons. In order for these enzymes to catalyze another reaction, $FADH_2$ must be oxidized to FAD.

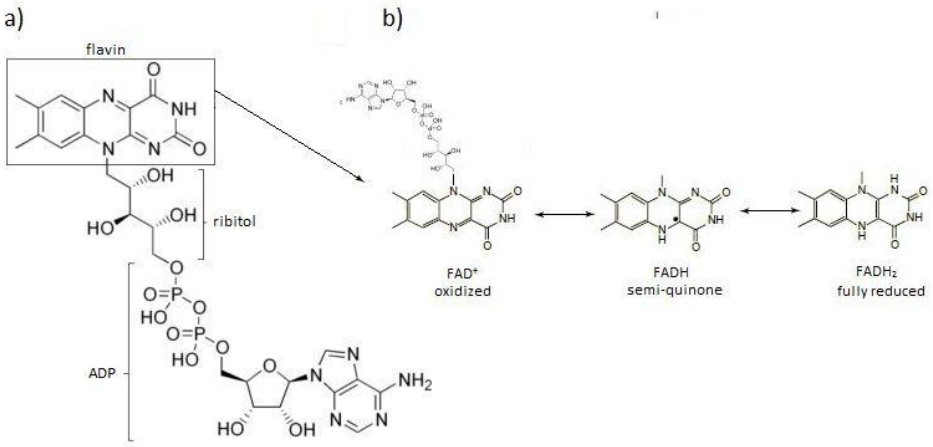

Figure 1.8 FAD structure and oxidation states. *The a) structure of FAD, indicating the flavin, ribitol and ADP regions and b) the three potential oxidation states of FAD going from fully oxidized to fully reduced.*

1.3.2 Electron transfer flavoprotein interacts with primary dehydrogenases

Multiple primary dehydrogenases involved in the metabolism utilize ETF as a shuttle, oxidizing the FAD group of the dehydrogenase and bringing the electrons to the ETF:QO. In this manner, the dehydrogenases are capable of performing multiple rounds of redox reactions while the electrons are used for ATP generation via the oxidative phosphorylation pathway. In effect, a cascade of redox reactions occurs that results in the electrons introduction to the quinone pool. The flow of electrons pass from substrate to dehydrogenase, then on to ETF followed by ETF:QO, and finally the quinone pool. The relationship between ETF and the primary dehydrogenases is vital, which becomes clear in cases of ETF or ETF:QO activity reduction. Reduced ETF or ETF:QO activity results in the reduced activity of many FAD-dependent dehydrogenases, leading to Glutaric Acidemia type II (GA II), also referred to as Multiple Acyl-CoA Dehydrogenase Deficiency (MADD). With reduced dehydrogenase activity, the inability to process their substrates results in metabolic acidosis (Frerman and Goodman, 1985). Dehydrogenases that interact with ETF include dehydrogenases involved in the 1-carbon metabolism of choline, which are the sarcosine and di-methyl glycine dehydrogenases (SARD and DMGD). It also interacts with dehydrogenases involved in amino acid catabolism, such as the isovaleryl-CoA and glutaryl-CoA dehydrogenases (IVD and GCD). Finally, ETF interacts

with dehydrogenases involved in the β-oxidation pathway of fatty acids, such as the medium chain fatty-acid dehydrogenase (MCAD)(Toogood et al., 2004).

1.3.3 Overview of metabolic pathways involved with electron transfer flavoprotein

MCAD is responsible for the initial step of the β-oxidation pathway, oxidizing medium chain acyl-CoA, resulting in the formation of a trans double bond between C2 and C3 (Thorpe and Kim, 1995). β-oxidation is a cyclic pathway in which two carbons are removed per cycle in the form of acetyl-CoA, which continues on to the citric acid cycle (figure 1.9a).

IVD is responsible for the oxidation of isovaleryl-CoA to 3-methylcrotonyl-CoA, the third step of leucine catabolism. Leucine is one of the branched-chain amino acids (BCAA), with catabolic pathways that are all quite similar but involving different enzymes (figure 1.9b). The end-products of Leucine degradation is acetoacetic acid and acetyl-CoA (Luís et al., 2011).

GCD is involved in the metabolism of lysine, hydroxyl-lysine and tryptophan. The initial steps of Lysine degradation in mammals differs slightly from the initial steps in *A. tumefaciens*, however later steps follow a common path. It is within the common pathway GCD is involved, oxidizing glutaryl-CoA to glutaconyl-CoA (figure1.9c)(de Mello Serrano et al., 2012; Misono and Nagasaki, 1982). The product of lysine degradation is acetyl-CoA.

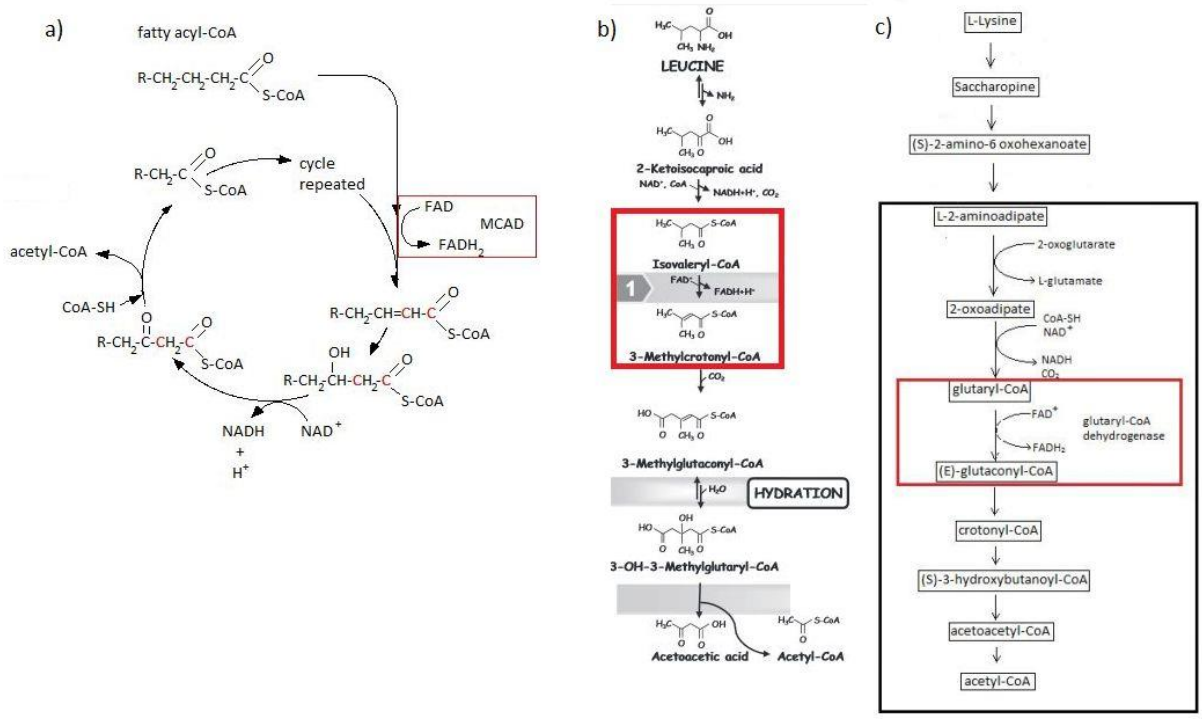

Figure 1.9 Metabolic pathways of ETF interacting dehydrogenases MCAD, IVD and GCD. *The a) catabolic pathway of fatty acids, in which MCAD is involved in the degradation of fatty acids with medium length chains (tails of 6-12 carbons in length). MCAD is involved in the process boxed in, leading to the formation of trans-Δ^2-enoyl-CoA from fatty acyl-CoA. The b) catabolic pathway for leucine, with the process IVD is involved in indicated. The c) catabolic pathway for lysine, with the pathway common to H.sapiens and A.tumefaciens in the large box and the process with which GCD is involved in the smaller box. For all three of these pathways the final product is acetyl-CoA, which continues through the citric acid cycle. Figure 1.9b adapted from (Luís et al., 2011).*

SARD and DMGD are both involved in the choline oxidation pathway. DMGD is involved in the formation of sarcosine, which is processed by SARD to glycine. Both dehydrogenases

contain a domain to which FAD covalently binds, but an additional contained domain links the metabolic pathway to the folate cycle by binding tetrahydrofolate (THF). The dehydrogenases utilizes formaldehyde removed from their substrate to form 5,10- methylene tetrahydrofolate (5,10-me THF) from its bound THF (Wittwer and Wagner, 1981). 5-meTHF in turn couples to the methionine cycle, donating the methyl group to homocysteine to form methionine. There are additional couplings to the folate and methionine cycles within the metabolic pathway for sarcosine (figure 1.10)(Blom and Smulders, 2011; Metallo, 2012).

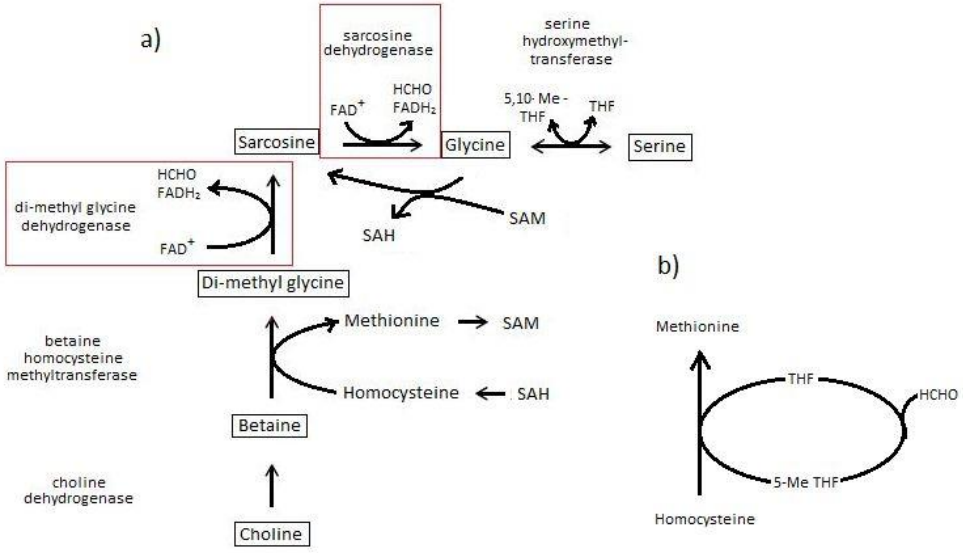

Figure 1.10 Metabolic pathways of ETF interacting dehydrogenases DMGD and SARD. *The a) catabolic pathway for choline, with the processes DMGD and SARD are involved in boxed. The HCHO bi-product links to the folate cycle, which in turn is involved in the methionine cycle. The b) generalized schematic in which the coupling between the dehydrogenases and folate cycle depicted as formaldehyde, as well as the coupling between the folate and methionine cycles.*

1.4 Model organisms

Model organisms are utilized to uncover information regarding the processes that together give life to living organisms. Model organisms are comprised of organisms ranging from mammals to prokaryotes as well as plants. Some common model organisms include *Mus musculus* (mouse), *Drosophila melanogaster* (fruit fly), *Saccharomyces cerevisiae* (budding yeast), *Schizosaccharomyces pombe* (fission yeast) and *Arabidopsis thaliana*.

In model organism selection, certain qualities making them advantageous in the laboratory must be present. Qualities such as small genome size, which increases the likelihood of the genome having been fully sequenced, as well as the organism itself being small and easy to handle. The organism should also have a short life cycle, as well as a rapid development, and should be easy to keep alive and handle. An important trait is the ability to perform genetic alterations and manipulations of the organism, such as the knocking out of genes. Finally, the cost of growing/maintaining the model organism is an important consideration.

1.4.1 Agrobacterium tumefaciens as model organism for study of METTL20 function

A. tumefaciens is a gram-negative alphaproteobacterium present in soil, and is a phytopathogen, responsible for crown gall in numerous plant species. The virulence of *A. tumefaciens* is only possible when the cells contain a 'tumour inducing' plasmid (Ti-plasmid). The Ti-plasmid contains a segment of T-DNA and the genes needed to express it, denoted 'plasmid localized virulence' (vir) genes. The T-DNA is transduced into the plant cell through the T-pilus. Once the T-DNA has entered the nucleus of the plant cell, it inserts randomly into the genome and expresses genes that lead to tumour formation, as well as disturbing the hormone balance in order to force the expression of opines in the plant cell that the bacterium uses as a source of energy (Li et al., 2000).

Reasons for choosing *A. tumefaciens* as a model organism include the size as well as ease of handling and growing, but the most important factor is the presence of an METTL20 orthologue. Utilizing the orthologous system, the function of METTL20 as well as potential biological role could be investigated. The entire genome of *A. tumefaciens* has been sequenced, which is beneficial in regards to cloning of genes. It was also not overly complicated to perform a gene knockout in *A. tumefaciens*, a vital step in the characterization.

1.5 Mobile group IIA introns

Group IIA introns are self-catalytic ribozymes present in all kingdoms of life. Aided by one or more intron-encoded proteins (IEPs) and sequence recognition within the intron, formation of a stable lariat occurs during the self-splicing process. The lariat encompasses six domains (DI to DVI), which are further subdivided as shown in figure 1.11.

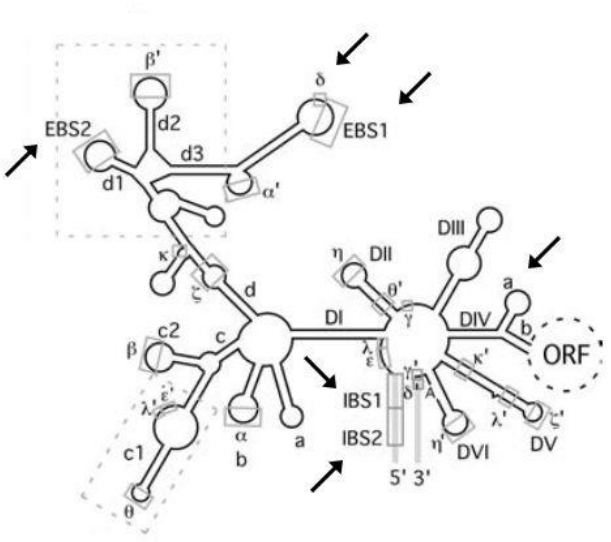

Figure 1.11 Intron lariat formed by group IIA introns. *Important regions of the lariat are indicated with arrows except for δ' due to its location in the figure. The lariat structure encompasses domains I to VI, further sub-divided using lower-case letters and numbers. The IBS1 and IBS2 on the flanking 5' exon form base pairs to the EBS1 and EBS2 sequences of the intron. The δ similarly base pairs to the δ' sequence of the flanking 3' exon. Domain IV, sub-domain a (DIVa) contains the high-affinity binding site for the IEP. Adapted from (Lambowitz and Zimmerly, 2004).*

Key regions involved in sequence recognition are intron-binding sites one and two (IBS1, IBS2) located on the flanking five prime-exon (5'-). These regions are complementary to exon-binding sites 1 and 2 (EBS1, EBS2). In this manner, the IBS regions form 5-6 base pairs with their recognized EBS sequences. In addition, group IIA introns contain a delta (δ) region adjacent to EBS1 that base-pairs with δ' located on the flanking three prime-exon (3'-). The stabilization helps positioning the splice junction at the ribozymes active site. An IEP binds the intron lariat which contains a high-affinity binding site in domain V-a, and aids in the formation of the catalytically active structure of the intron. The catalytically active intron and bound IEP form a ribonucleoprotein (RNP). The RNPs binding specificity for targets is in part due to the IEP, but mainly as a result of the EBS sequences which base pair with complementary sequences in target DNA or RNA. The IEP carries additional functions other than stabilization of the intron, including endonuclease activity and reverse transcriptase activity. IEP is also responsible for local DNA unwinding allowing the EBS regions to base pair with their target DNA. A number of suggested mechanisms exist for the mobility of the introns as well as the exact mechanism of intron insertion into the target DNA/RNA. The generalized mechanism is the cleavage of either one or both strands of the DNA, followed by either homologous recombination of a cDNA of the intron or insertion of the intron followed by reverse transcription using the targets DNA as primer and intron as template (Lambowitz and Zimmerly, 2004).

1.5.1 Generation of knockout bacteria using the TargeTron system

The TargeTron system from Sigma-Aldrich makes use of mobile group II introns in order to insert introns into a gene of interest (GOI), disrupting the gene. The intron introduces a stop codon downstream of the intron insertion site, generating a truncated protein when translated. The truncated protein is generally non-functional, and so the wild type (WT) activity of the encoded protein is lost in the cells carrying the disrupted gene. The mechanism functions by using a trademarked algorithm that finds potential binding sites for the RNP, and generates primers to alter the EBS1, EBS2 and δ so that they recognize sequences within the GOI. Another primer also alters IBS1 and IBS2, so that the ability to form base pairs with EBS1 and EBS2 during the initial lariat formation remains. In this manner, the lariat is ensured to assume the correct structure during splicing. The TargeTron system uses the *Lactococcus lactis* L1.LtrB group IIA intron, which is comprised of the LtrB intron and LtrA IEP (hereafter referred to as the TargeTron cassette). L1.LtrB functions by insertion of the intron followed by reverse transcription of the intron by the IEP to produce cDNA, after which the hosts own repair machinery removes the intron RNA and replaces it with DNA complementary to the introns' reverse transcribed cDNA. The host is also responsible for the ligation reaction (figure 1.12a)(Cousineau et al., 1998). The TargeTron cassette has been cloned into several vectors, allowing expression of the intron and IEP from a variety of organisms. This allows the use of the system with a wide variety of organisms, as the cassette can be cloned into a vector containing promoters and selection markers suitable for the target organism. The pBL1 plasmid was created by cloning of the TargeTron cassette downstream of the m-toluic acid inducible XylS gene of the pJB866 vector, a positive regulator of the promoter (Blatny et al., 1997). Use

of pBL1 is proven to function in a variety of gram-negative bacteria, including *A. tumefaciens*. It contains a tetracycline (Tet) antibiotic marker (figure 1.12b)(Yao and Lambowitz, 2007).

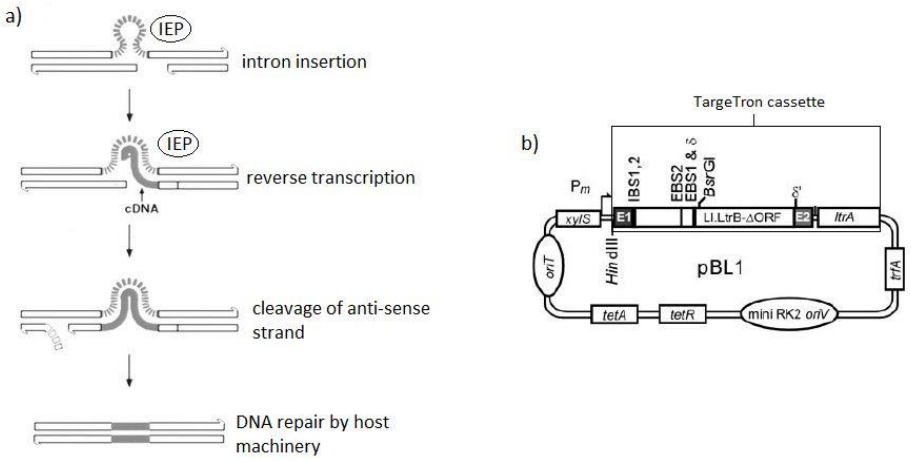

Figure 1.12 pBL1 plasmid containing TargeTron cassette and intron insertion into the GOI. *a) The mechanism of intron insertion by L1.LtrB group IIA introns, in which the intron inserts into the sense strand. The IEP reverse transcribes a cDNA anti-sense strand which is the template used by the hosts own DNA repair machinery. Adapted from (Cousineau et al., 1998). b) The pBL1 vector containing the TargeTron cassette inserted into pJB866 behind the m-toluic acid inducible promoter xylS. pBL1 contains a tetracycline resistance marker. The regions targeted by the TargeTron primers IBS, EBS1|δ and EBS2 shown, located between the HindIII and BsrGI restriction sites. Adapted from (Yao and Lambowitz, 2007).*

The system together with the pBL1 vector allow for easy retargeting of the intron. The regions recognized by the retargeting primers are located between HindIII and BsrGI restriction sites. As a result, retargeting PCR can be performed on just the fragment between these sites followed by ligation back into the vector after digestion with the restriction enzymes.

1.6 pET28a- plasmid for overexpression of His-tagged proteins in *Escherichia coli*

The pET28a vector is commonly used for overexpression of recombinant proteins from *E. coli*. The cloning site of the vector contains multiple restriction sites, allowing the use of a variety of restriction enzymes for cloning. The vector is generally used in *E. coli*, using the kanamycin (Km) antibiotic selective marker to validate the uptake of the vector by the host organism.

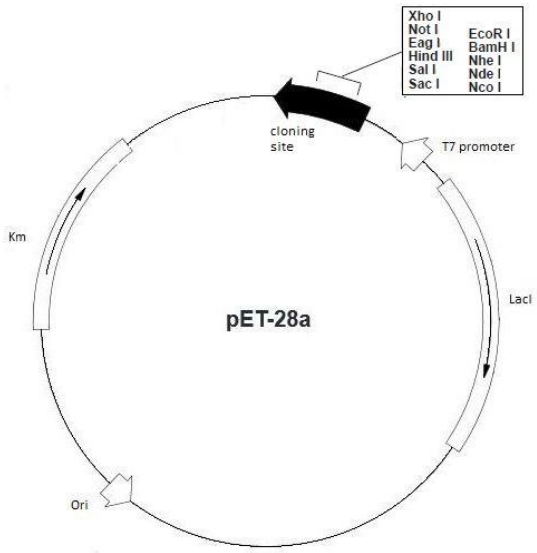

Figure 1.13 pET28a vector map. *Black arrow indicating the cloning site, with restriction sites indicated. T7 promoter with lac operator (not shown), repressed if the lac repressor (lacI) is expressed. IPTG stimulation inhibits the expression of the lac repressor, resulting in overexpression by the T7 RNA polymerase. Km antibiotic selective marker. The origin (Ori) of replication ensures replication of the vector in the host.*

E. coli strains such as BL21 DE3 contain the gene for T7 RNA polymerase, which is necessary for expression from pET28a as the cloning site is downstream of a T7 promoter. Overexpression is achieved by addition of isopropyl β-D-1-thiogalactopyr (IPTG), which mimics allolactose and binds the gene for the lacI repressor of pET28a hindering its expression. Unlike allolactose, IPTG is not broken down. This leads to continuous expression as the lac operator no longer is repressed. pET28a allows the expression of recombinant protein with an N-terminal hexa histidine-tag (6XHis-tag), as well as an optional C-terminal His-tag. A thrombin cleavage site situated between the His-tag and cloning site allows for the removal of the His-tag, if desired.

2. Aim of Study

The overall aim of this study was to characterize the novel human MTase METTL20. Prior to my engagement, potential substrates had been identified by mass spectrometry (MS). The following list addresses the particular goals it was desired to achieve;

1. Verify the identified substrates as true substrates of METTL20.
2. Experimentally determine the residues of the substrate methylated by METTL20.
3. Generate a strain of *A. tumefaciens* with a knockout of the METTL20 orthologue.
4. Uncover the biological function of METTL20 by comparison of the wild type (WT) and knockout (KO) *A. tumefaciens* strains.

3. Materials and Methods

3.2 Chemicals

Common laboratory chemicals from Sigma-Aldrich, Merck, BD Biosciences, Invitrogen and VWR. Antibiotics including tetracycline, kanamycin, rifampicin, chloramphenicol and gentamycin from Sigma-Aldrich. L-amino acids including lysine, leucine and glutamic acid from Sigma-Aldrich. IPTG, ponceau S, triton X-100, ethidium bromide, sarcosine, kosher octonoic acid (octonoate), betaine, choline chloride, 2-mercaptoethanol and m-toluic acid from Sigma-Aldrich. Bacto yeast extract and tryptone from BD Biosciences. EN3HANCE spray and S-adenosyl-L-[methyl-3H] methionine (250uCi) from Perkin Elmer. Loading buffer for DNA gel electrophoresis, deoxynucleotide triphosphates (dNTPs) and GeneRuler 1kb Plus DNA ladder from Thermo Scientific. NuPAGE MES buffer and transfer buffer from LifeTechnologies. Precision-Plus dual-color protein ladder from Bio-Rad. Nuclease-free water from Promega. Ni-NTA agarose from Qiagen. Complete protease inhibitor cocktail tablets from Roche. D-mannitol was a kind gift from Professor K.K. Andersson. Biotin was a kind gift from Professor D. Klaveness.

3.3 Materials

Cloning primers ordered from LifeTechnologies. Mutational cloning primers designed using PrimerX (appendix I), primers ordered from LifeTechnologies. TargeTron METTL20 KO primers designed using Sigma-Aldrich TargeTron Design Site (appendix I), primers ordered from LifeTechnologies. Universal retargeting primer from TargeTron Gene Knockout System, Sigma Aldrich.

GoTaq DNA polymerase and Green GoTaq buffer from Promega. Phusion HF DNA polymerase and Phusion buffer from Finnzymes. T4 DNA ligase and ligase buffer from NewEngland BioLabs. NdeI, HindIII, BsrGI and BamHI restriction enzymes as well as buffers from NewEngland BioLabs. Benzonase nuclease from Sigma-Aldrich. Recombinant 6XHis-tagged *A. tumefaciens* METTL20 MTase was a kind gift from Dr. J. Malecki.

The pET28a plasmid from EMD Millipore. The pBL1 plasmid from the Lambowitz lab.

E. coli DH5α competent cells from LifeTechnologies. *E. coli* BL21 DE3 RIPL competent overexpression cells from Agilent Technologies. *A. tumefaciens* C58 and GV3101 pM90 cells were kind gifts from Dr. P. Grini. *A. tumefaciens* C58 DNA from ATCC.

NucleoSpin Gel and PCR Clean-up kit and NucleoSpin Plasmid kit from Machery-Nagel. BCA Protein assay kit from Pierce. TargeTron kit from Sigma-Aldrich.

NuPAGE Novex 4-12% Bis-Tris pre-cast gels, SimplyBlue Safestain and polyvinylidene difluoride membranes from LifeTechnologies. Carestream Kodak BioMax MS X-ray film from Sigma-Aldrich. Oxoid AnaeroGen system kindly lent to me by Dr. Å.K. Røhr

3.4 Cloning

Amplification of genes performed by running PCR using Phusion HF DNA polymerase and gene cloning primers with purified *A. tumefaciens* C58 DNA as template. Reaction mixes prepared according to Phusion PCR protocol. PCR run using the Phusion PCR program (table 3.1). PCR product run through 1% agarose gel DNA electrophoresis, band of correct size cut from gel and purified using NucleoSpin Gel and PCR Clean-Up kit according to protocol. DNA concentration measured by Nano-Drop at 260nm. Purified PCR products digested according to protocol for the restriction enzymes used. Digested PCR products run through 1% agarose gel DNA electrophoresis and purified as before. DNA concentration measured as before. Fragments ligated into digested pET28a using T4 DNA ligase, followed by transformation into *E.coli* DH5α competent cells according to the T4 ligation protocol. Ligation mixes plated on LB plates (per liter: 10g tryptone, 5g yeast extract, 10g NaCl, 1.5% bacto agar) with 50 µg/mL kanamycin (Km). Transformants screened by colony PCR with GoTaq DNA polymerase. Reaction mix for colony PCR set up according to GoTaq protocol, and run on GoTaq PCR program (table 3.2). Successful transformants grown in 20mL LB medium (medium as for LB plates, without bacto agar) complemented with 50 µg/mL Km overnight at 37°C with rigorous shaking. Plasmid purification performed of overnight culture using NucleoSpin Plasmid kit according to protocol for low-copy plasmid isolation. Purified plasmid used as template for sequencing with primers for pET28a sequencing, including fwd primer (ATGCGTCCGGCGTAGAGG) that binds upstream of the T7 promoter region and rev primer (TAGAGGCCCCAAGGGGTTATGCTAG) that binds at the T7 terminator region.

Table 3.1 Phusion PCR program

Step	Cycles	Time	Temperature
Initial denaturation	1	30 seconds	98 ° C
Denaturation	35	10 seconds	98 ° C
Annealing	35	15 seconds	50 ° C
Elongation	35	15 seconds / kbp	72 ° C
Final elongation	1	10 minutes	72 ° C
Holding	1	∞	4 ° C

Table 3.2 GoTaq PCR program

Step	Cycles	Time	Temperature
Initial denaturation	1	2 minutes	95 ° C
Denaturation	35	30 seconds	95 ° C
Annealing	35	30 seconds	50 ° C
Elongation	35	1 minute / kbp	72 ° C
Final elongation	1	5 minutes	72 ° C

3.5 Mutagenesis

Mutagenesis of cloned genes performed in same manner as cloning but in a two-step process. First step performed with two reactions using purified insert-containing pET28a as template. One reaction contained fwd gene cloning primer and rev mutational primer. Second reaction contained rev gene cloning primer and fwd mutational primer. PCR products of both reactions

purified and together used as templates in sewing PCR with fwd and rev cloning primers to generate full-length clones with introduced mutations. Generalized mechanism of two-step mutagenesis PCR shown in figure 3.1.

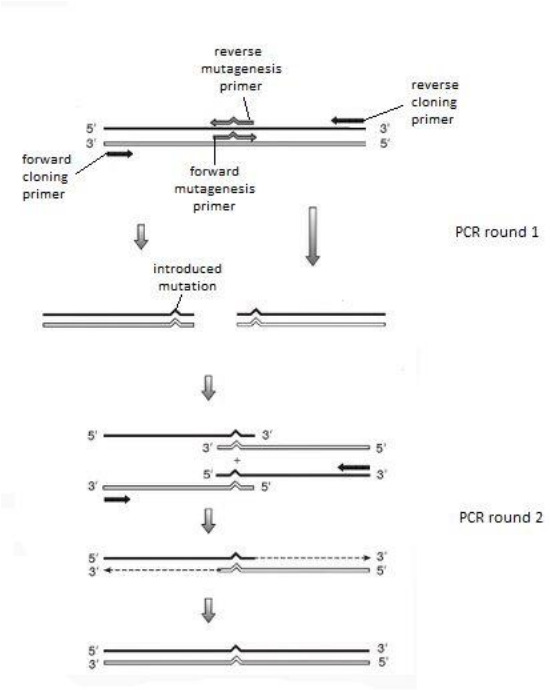

Figure 3.1 Two-step mutagenesis PCR. *The general mechanism of mutagenesis using two-step PCR. The first step makes use of both the gene cloning primers and mutagenesis primers to generate the template used in the second round of PCR. In the second round, only the gene cloning primers are used in order to PCR the full-length PCR product including the introduced mutations.*

3.6 Expression of recombinant protein and purification

Plasmids containing gene clones and mutants sequenced using the gene cloning primers by the ABI lab, and analyzed using Sequencher (appendix I). Sequenced plasmids transformed into *E. coli* BL21 DE3 RIPL expression strain cells according to manufacturer's protocol, and plated on LB plates with Km. Transformants verified by colony PCR screening using the gene cloning primers. Successfully transformed BL21 DE3 RIPL cells grown in overnight culture with Km and 34 µg/mL chloramphenicol (Cm) before transferal to 500mL terrific broth (TB)(per liter: 5g beef extract, 1g yeast extract, 5g peptone, 5g sucrose, 0.5g $MgCl_2$). TB supplied with Km and Cm and grown at 37°C with rigorous shaking until reaching an OD600 of 0.7-1.0. Once appropriate OD600 reached, temperature lowered to 16°C and 0.1mM IPTG added to induce overexpression of recombinant protein. Expression cultures grown overnight. Cells harvested by centrifugation (6000 times gravity) at 4°C in a JA-10 rotor for 12 minutes. Harvested cells resuspended in **lysis buffer**: buffer A (50mM NaH_2PO_4 pH7.2, 5% glycerol, 2mM β-mercaptoethanol) supplemented with 300mM NaCl, 1% triton X-100, 1X Complete protease inhibitor cocktail and benzonase. Resuspension sonicated and centrifuged (20,000rpm) at 4°C in a JA25.5 rotor for 30 minutes. Supernatant filtered through a sterile 0.45µm filter. PolyPrep Chromotography column with added 0.7mL Ni-NTA agarose equilibrated in **wash buffer 1**: buffer A, supplemented with 300mM NaCl, 1% triton X-100, and 20mM imidazole. Filtered lysate added in order to purify recombinant His-tagged protein. Column washed with wash

buffer 1 (10X column volume), followed by **wash buffer 2**: buffer A, supplemented with 2M NaCl, 1% triton X-100 and 20 mM imidazole (5X column volume). Final wash with **wash buffer 3**: buffer A complemented with 300 mM NaCl and 20 mM imidazole (10X column volume). Proteins bound to Ni-NTA resign eluted with **elution buffer**: buffer A, supplemented with 300 mM NaCl and 200mM imidazole (3X column volume). Eluted fractions measured using Nanodrop at 280nm. Fractions containing protein pooled and dialyzed in VivaSpin 20 centrifugal concentrators in **storage buffer** (50mM Tris-HCl pH 7.6, 50mM KCl, 2mM dithiothreitol (DTT), 5% glycerol). Protein purity was ascertained by running SDS-PAGE of dialyzed protein samples alongside the Precision-Plus dual-color protein ladder, using NuPAGE pre-cast gels in 1X SDS-PAGE running buffer (per liter: 3.02g Tris, 14.4g glycine,1g SDS) according to NuPAGE protocol. Gels stained using SimplyBlue safestain according to protocol. Quanititation of protein performed using BCA Protein Assay kit following the protocol for microplates.

3.7 Methyltransferase assay

Reactions set up in 10µL volumes, containing 100pmol recombinant protein substrate, 40pmol enzyme and 6.6pmol S-adenosyl-L-[methyl-3H] methionine (3H-SAM) in storage buffer. Reaction mixes incubated 28°C for 2 hours. SDS-PAGE run as previously, followed by transferal of protein to a polyvinylidene difluoride (PVDF) membrane using XCell II blot module from LifeTechnologies according to protocol. Membrane stained with ponceau S containing 5% acetic acid and de-stained using 2.5% acetic acid. Prior to fluorography, membrane sprayed with EN3HANCE spray according to protocol. Membrane incubated in a sealed folder against a BioMax MS film at -80°C overnight.

3.8 Generation of competent *A.tumefaciens* GV3101 pM90 cells

Culture of *A.tumefaciens* started in 5mL YEB medium (per liter: 5g beef extract, 1g yeast extract, 5g peptone, 5g sucrose, 0.5g $MgCl_2$) complemented with 50 µg/mL rifampicin (Rif), 50 µg/mL gentamycin (Gent) and 50 µg/mL Km. Overnight growth, 28°C with shaking. 2mL overnight culture added to 50mL YEB medium supplemented with Rif, Gent and Km. Incubated 28°C with shaking until OD600 0.5-1.9 attained. Culture chilled on ice, followed by 5 minute centrifugation (3,000 times gravity) at 4°C. Harvested cells resuspended in 1mL ice-cold 20 mM $CaCl_2$ solution. Aliquoted in 100 µL volumes and frozen in liquid nitrogen.

3.9 Generation of *A.tumefaciens* METTL20 gene knockout

Primers for retargeting the intron towards METTL20 of *A. tumefaciens* C58 designed using TargeTron design site. Retargeting PCR performed in two-steps by Dr. Malecki in the same manner as performed for mutagenesis. Primers designed shown with the retargeted sequence in bold and underlined; EBS1|δ (CAGATTGTACAAATGTGGTGATAACAGATAAGTC**<u>TCCGGTCT</u>** TAACTTACCTTTCTTTGT), EBS2 (TGAACGCAAGTTTCTAATTTCG**<u>ATTCCACT</u>**TCGATAGAGGAA AGTGTCT), IBS (AAAAAAGCTTATAATTATCCTTA**<u>AGTGGCTCCGGT</u>**GTGCGCCCAGATAGGGTG). First reaction run with fwd primer IBS and universal rev primer (CGAAATTAGAAAC TTGCGTTCAGTAAAC) from the TargeTron kit. Second reaction run with fwd primer EBS2 and rev primer EBS1|δ. Purified pBL1 plasmid used as template in reactions. PCR products of both reactions purified and together used as template for sewing PCR, utilizing fwd primer IBS and

rev primer EBS1|δ. Second round PCR product was full-length retargeting region of intron, which lies between the HindIII and BsrGI restriction sites (see figure 1.12b). Restriction digestion, ligation, and transformation into DH5α performed as in gene cloning. Colony PCR of DH5α containing pBL1 performed with fwd primer IBS and rev primer EBS1|δ. Plasmid purification as in gene cloning, and sequencing performed with same primers as in colony PCR. pBL1 verified by sequencing transformed into *A. tumefaciens* GV3101 pM90 competent cells. Aliquot of competent GV3101 pM90 cells thawed on ice and 0.2µg pBL1 plasmid mixed into cells. Cells frozen at -80°C and thawed by 5 minutes in water bath, followed by incubation on ice for 30 minutes. 100µL LB without antibiotics added and cells incubated at 28°C with shaking for 30 minutes. Cells plated on pre-warmed (28°C) LB plates complemented with Rif, Gent and 12.5 µg/mL Tet. These antibiotics used as *A. tumefaciens* GV3101 pM90 transformed with pBL1 carries Rif resistance in genomic DNA, Gent resistance in helper plasmid and Tet resistance from pBL1. Plates incubated at 28°C. Colony PCR performed using fwd primer IBS and rev primer EbS1|δ. Successful transformants grown in MG/L medium pH 7.0 (per liter: 5g D-mannitol, 1g L-glutamic acid, 250mg KH_2PO_4, 100mg NaCl, 100mg $MgSO_4$ heptahydrate, 5g tryptone, 2.5g yeast extract, 1µg biotin) with antibiotics at 28°C with shaking. Induction performed at OD600 0.3-0.4 with 5mM m-toluic acid. Cells grown 3 hours at 30°C with shaking. Cells harvested by centrifugation as in protein expression, and resuspended in MG/L medium containing antibiotics. Cells plated on MG/L plates (MG/L medium with 1.5% bacto agar) supplemented with antibiotics. Colony PCR screening performed to identify METTL20 genes with 900bp intron insertion. Performed using gene cloning primers for *A. tumefaciens* C58 METTL20 designed by Dr. Malecki, with fwd primer (ACTACTGGCATATGAGGACCGATCC CGAGCGCTTC) and rev primer (ATGTAGACGGATCCTCAGATAAAACGCCACACCGTGGTC).

Curing of pBL1 from *A. tumefaciens* GV3101 pM90 with intron insertion in METTL20 gene performed by growth of colonies identified in colony PCR in LB medium supplemented with Rif and Gent, but no Tet. Cultures grown overnight at 28°C with shaking. Overnight cultures plated on LB plates containing Rif and Gent. Clones sensitive to Tet screened by colony PCR for presence of METTL20 gene with intron insertion. Functional assays run to test these cells of *A. tumefaciens* GV3101 pM90 with the METTL20 gene knocked out (*A. tumefaciens* METTL20 KO).

3.10 Assessing METTL20 function utilizing different growth conditions

Growth comparisons performed utilizing the *A. tumefaciens* METTL20 KO strain, comparing growth to the *A. tumefaciens* GV3101 pM90 strain used to make competent cells (*A. tumefaciens* METTL20 WT). METTL20 function assessed by comparing ability of these strains to grow under various growth conditions. Unless otherwise specified, growth ascertained by measuring OD600 of cultures while growing at 28°C (with shaking for liquid medium). Initial amounts of cells used to start cultures determined by OD600, and were grown in cultures of either YEB or M9 medium (per liter: 8.54g Na_2HPO_4 dihydrate, 3g KH_2PO_4, 0.5g NaCl, 1g NH_4Cl, 1mM $MgSO_4$, 100µM $CaCl_2$, $3x10^{-9}$M $(NH_4)_6Mo_7O_{24}$ tetrahydrate, $4x10^{-7}$M H_3BO_3, $3x10^{-8}$M $CoCl_2$ hexahydrate, $1x10^{-8}$M $CuSO_4$ pentahydrate, $8x10^{-8}$M $MnCl_2$ tetrahydrate, $8x10^{-8}$M $ZnSO_4$ heptahydrate, 1µM $FeSO_4$ heptahydrate) supplemented with Rif and Gent. Cultures started with identical amounts of *A. tumefaciens* GV3101 pM90 WT and

METTL20 KO cells and grown in YEB or M9 medium supplemented with Rif and Gent. M9 medium contained glucose (22.2mM), lysine (200µM), leucine (400 µM), octonoic acid (500 µM), choline (10mM), betaine (10mM) or sarcosine (10mM) as sole carbon source. Combinations of lysine, leucine and glucose also used at same concentrations.

A. tumefaciens METTL20 WT and KO strains also subjected to stress conditions in order to compare growth under stress. In order to test for growth under oxidative stress, cells grown in media supplemented with 2mM H_2O_2 for 15 minutes. In order to test for growth under anaerobic conditions, cells grown on YEB plates incubated in chamber deprived of oxygen using Oxoid Anaerogen system, according to protocol. In order to test growth under osmotic stress, growth medium supplemented with 0.3M-0.7M NaCl. In order to test growth under heat-shock, cells subjected to increasing temperatures for various amounts of time. To test the viability of cells grown under different stress conditions, the cell cultures were typically placed back into optimal growing conditions (28°C, medium without stress compound, normal areation) and tested for the ability to form colonies (cultures on plates) and/or sustain growth as judged by measuring OD600 (liquid cultures).

4. Results

4.1 RpL7/L12 is a substrate of *A. tumefaciens* METTL20

RpL7/L12 was identified as a putative substrate in lysates from *A. tumefaciens* C58 by MS analysis by other members of the Falnes group. In order to verify this preliminary finding, the gene for RpL7/L12 (RefSeq: NP_354932.1) was cloned using the fwd gene cloning primer (ACTACTGG**CATATG**GCTGATCTCGCAAAGATCG) and rev gene cloning primer (ATGTAGA C**GGATCC**TTACTTAACGTCGACCTTGGCG). Nucleotides in bold and underlined indicate sequences recognized by restriction enzymes. Purified digested PCR products were inserted into pET28a between the NdeI and BamHI restriction sites. Recombinant RpL7/L12 protein was expressed with a 6XHis-tag and purified. Purified recombinant protein was used in an MTase assay reaction together with recombinant *A. tumefaciens* METTL20. The negative controls included a reaction in which only METTL20, and a reaction in which only RpL7/L12 was present. All reactions were incubated in the presence of 3H-SAM. Incorporation of the 3H-labelled methyl groups was visualized using fluorography after SDS-PAGE and transferal to a PVDF membrane. As can be seen in figure 4.1, a strong methylation band is present when METTL20 and RpL7/L12 are present in the same reaction mixture. RpL7/L12 alone gave no band, and METTL20 alone gave a visible but weaker band.

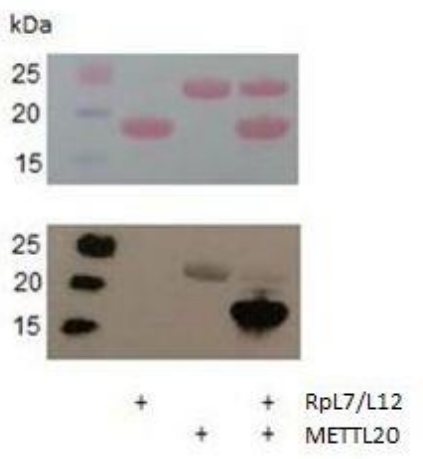

Figure 4.1 Methylation of recombinant RpL7/L12 by recombinant METTL20. *Reactions, containing proteins as indicated, were incubated with 3H-SAM (see Mat. and Meth.) and analyzed by SDS-PAGE followed by transfer of proteins to PVDF membrane. The membrane was stained with Ponceau S (upper panel) and exposed to X-ray film for fluorography (lower panel). The position of markers is shown on the left*

Based on these results, one may conclude that RPL7/L12 is efficiently being methylated by METTL20 in the presence of SAM. Therefore, it represents a true substrate for methylation by METTL20 in vitro. In addition, METTL20 appears to perform automethylation. This automethylation is severely reduced when the true substrate, RpL7/L12, is present.

4.2 METTL20 methylates residue K86 of RpL7/L12

Samples of RpL7/L12 were prepared and sent in for MS analysis by other members of the group. This identified lysine 86 (K86) as the putative site of methylation. In order to verify that this was the true site of methylation by METTL20, a similar experiment was performed as for RpL7/L12 but with a mutation of K86 to alanine (A) in RpL7/L12 (RpL7/L12 K86A). In order to generate the RpL7/L12 K86A mutant, two-step PCR was performed, using the fwd mutational primer (GGGTCTCGGCCTG**GC**GGAAGCTAAGGAC) and rev mutational primer (GTCC TTAGCTTCC**GC**CAGGCCGAGACCC), together with the gene cloning primers for RpL7/L12. Purified pET28a-RpL7/L12 was used as template. The nucleotides of the primers in bold and underlined indicate the nucleotides that are mutated in respect to the RpL7/L12 sequence in order to introduce the desired amino acid substitution. The same restriction sites as for RpL7/L12 were used for pET28a insertion. The RpL7/L12 K86A recombinant protein was expressed and purified. The MTase assay reaction and visualization was performed as for RpL7/L12 but with the addition of RpL7/L12 K86A, as well as a negative control containing RpL7/L12 K86A but no METTL20. RpL7/L12 with METTL20 was the positive control. As can be seen in figure 4.2, a strong methylation band was present when RpL7/L12 and METTL20 were present in the same reaction, however the RpL7/L12 K86A mutation did not result in any bands even in the presence of METTL20. The negative controls gave no bands, except for the reaction in which only METTL20 was present.

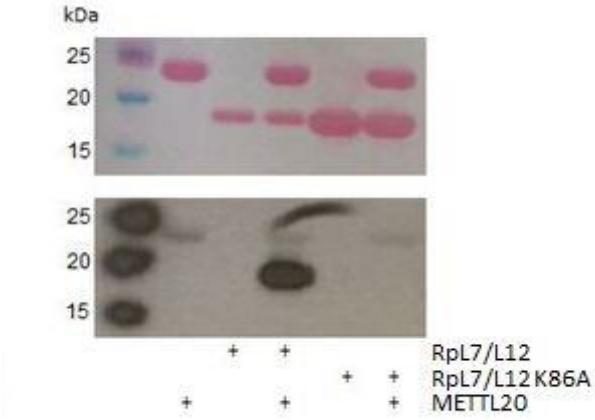

Figure 4.2 Methylation of recombinant RpL7/L12 K86A mutant by recombinant METTL20. *Reactions, containing proteins as indicated, were incubated with 3H-SAM (see Mat. and Meth.) and analyzed by SDS-PAGE followed by transfer of proteins to PVDF membrane. The membrane was stained with Ponceau S (upper panel) and exposed to X-ray film for fluorography (lower panel). The position of markers is shown on the left*

Based on these results, one may conclude that K86 is the residue that is being methylated, as mutation of this residue to alanine abolished the methylation band produced by RpL7/L12 in the presence of SAM. Therefore, it represents a true site of methylation by METTL20 in vitro. Once again, automethylation of METTL20 was observed.

4.3 ETFβ is a second substrate of METTL20

ETFβ was identified as a putative substrate in lysates from *A. tumefaciens* C58 by MS analysis by other members of the Falnes group. In order to verify this preliminary finding, the gene for ETFβ (RefSeq: NP_357017.1) was cloned using the fwd gene cloning primer (ACTACTG G**CATATG**AAAATCCTTGTCCCCGTTAAACG) and rev gene cloning primer (ATGTAGA C**AAGCTT**AGAGGACGCCGTCGGC). The purified restriction digested PCR products were ligated into pET28a between the NdeI and HindIII restriction sites. Recombinant ETFβ protein was expressed with a 6XHis-tag and purified. In the same manner as performed for RpL7/L12, purified recombinant ETFβ was used in an MTase assay, which was visualized by fluorography. *H. sapiens* recombinant ETFβ1 designed, expressed and purified by Dr. Malecki was also tested as a substrate. Negative controls included METTL20 without substrate, ETFβ without enzyme and ETFβ1 without enzyme. As can be seen in figure 4.3, strong methylation bands were found for both *A. tumefaciens* ETFβ and *H. sapiens* ETFβ1 when METTL20 was present. Substrates alone gave no methylation band, METTL20 alone gave weak methylation bands barely visible in the image scan.

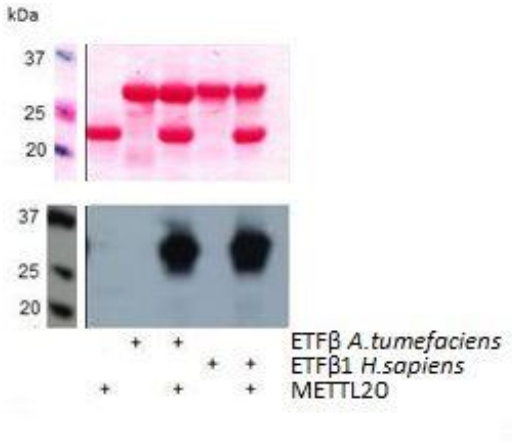

Figure 4.3 Methylation of recombinant A.tumefaciens ETFβ and H.sapiens ETFβ1 by recombinant METTL20. *Reactions, containing proteins as indicated, were incubated with 3H-SAM (see Mat. and Meth.) and analyzed by SDS-PAGE followed by transfer of proteins to PVDF membrane. The membrane was stained with Ponceau S (upper panel) and exposed to X-ray film for fluorography (lower panel). The position of markers is shown on the left.*

Based on these results, one may conclude that ETFβ as well as ETFβ1 are efficiently being methylated by METTL20 in the presence of SAM. Therefore, it represents another true substrate for methylation by METTL20 in vitro.

4.4 METTL20 methylates residues K193 and K196 of ETFβ

Samples of ETFβ were prepared and sent in for MS analysis by other members of the group. This identified lysine 193 (K193) as the putative site of methylation. In order to verify that this was the true site of methylation by METTL20, a similar experiment was performed as for RpL7/L12 K86A, in which K193 of ETFβ was mutated to an alanine and arginine (ETFβ K193A and ETFβ K193R). In order to generate the ETFβ K193A and ETFβ K193R mutants,

two-step PCR was performed using the ETFβ gene cloning primers together with the mutational primers. For ETFβ K193A, the mutational primers included the fwd mutational primer (GCTG CCGAACATCATG**GCG**GCAAAAAAGAAGCC) and rev mutational primer (GGCTTCTTTTTT GC**CGC**CATGATGTTCGGCAGC). For ETFβ K193R, the mutational primers included the fwd mutational primer (GCTGCCGAACATCATG**GCT**GCAAAAAAGAAGCCG) and rev mutational primer (CGGCTTCTTTTTTGC**AGC**CATGATGTTCGGCAGC). Purified pET28a-ETFβ was used as template. The PCR product was inserted into pET28a using same restriction enzymes as for ETFβ. The recombinant mutants were expressed and purified. The MTase assay reaction and visualization was performed as for ETFβ but with the addition of the two mutants. ETFβ1 was not used in this experiment. Negative controls included reactions containing enzyme with no substrate, and substrates with no enzyme. ETFβ with METTL20 was a positive control. As can be seen from figure 4.4, METTL20 together with ETFβ produced a strong methylation band. Neither the ETFβ K193A or ETFβ K193R mutations abolished the methylation bands of WT ETFβ. Controls did not produce methylation bands, except the reaction with METTL20 alone, which gave a weak methylation band.

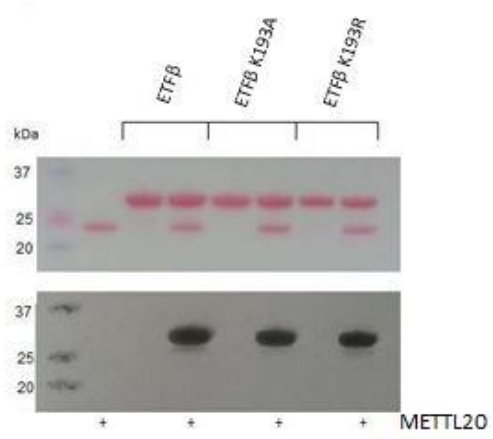

Figure 4.4 Methylation of recombinant ETFβ K193A and ETFβ K193R by recombinant METTL20. *Reactions, containing proteins as indicated, were incubated with 3H-SAM (see Mat. and Meth.) and analyzed by SDS-PAGE followed by transfer of proteins to PVDF membrane. The membrane was stained with Ponceau S (upper panel) and exposed to X-ray film for fluorography (lower panel). The position of markers is shown on the left*

Unexpectedly, both mutants were still methylated by METTL20. This could be explained by the fact that K193 was incorrectly identified as the methylation site. Alternatively, such a result could indicate that ETFβ contains more than one methylation site, in addition to K193. Indeed, further analysis of samples containing methylated human ETFβ1, suggested that both K200 and K203 are being methylated (Malecki et al., unpublished). These residues correspond to K193 and K196 of the *A. tumefaciens* ETFβ (figure 4.5).

Figure 4.5 Sequence alignment of H.sapiens ETFβ1and A.tumefaciens METTL20 methylation sites. *Region of sequence alignment with A.tumefaciens ETFβ (RefSeq: NP_357017.1) and H.sapiens ETFβ1 (RefSeq: NP_001976.1) containing the putative METTL20 methylation sites. Alignment performed with MUSCLE (Edgar, 2004)*

To verify K193 and K196 as the sites of methylation, two additional mutants of ETFβ were prepared. The mutants generated were the ETFβ K196A mutant and ETFβ K193A/K196A double mutant. These mutants were cloned in the same manner as ETFβ K193A. Mutational cloning primers for ETFβ K196A included the fwd mutational primer (CATGAAGGCAAAA**GCG**AAGCCGCTCGACAAAAAG) and rev mutational primer (GCGGCTT**CGC**TTTTGCCTTCATGATGTTCGGCAG). Mutational cloning primers for ETFβ K193A/K196A included the fwd mutational primer (CATG**GCG**GCAAAA**GCG**AAGCCGCTCGACAAAAAG) and rev mutational primer (GCGGCTT**CGC**TTTTGC**CGC**CATGATGTTCGGCAG). Purified pET28a-ETFβ was used as template. The PCR product was inserted into pET28a using same restriction enzymes as for ETFβ. The recombinant mutants were expressed and purified. The MTase assay reaction and visualization was performed as for ETFβ but with the addition of the two mutants. ETFβ1 was not used in this experiment. Negative controls included reactions containing enzyme with no substrate, and substrates with no enzyme. ETFβ with METTL20 was a positive control. As can be seen in figure 4.6, only the ETFβ K193A/K196A double mutation fully abolished the methylation band produced by ETFβ by METTL20. Methylation bands appeared to be weaker for reactions containing METTL20 and ETFβ K193A or ETFβ K196A, in comparison to METTL20 and ETFβ.

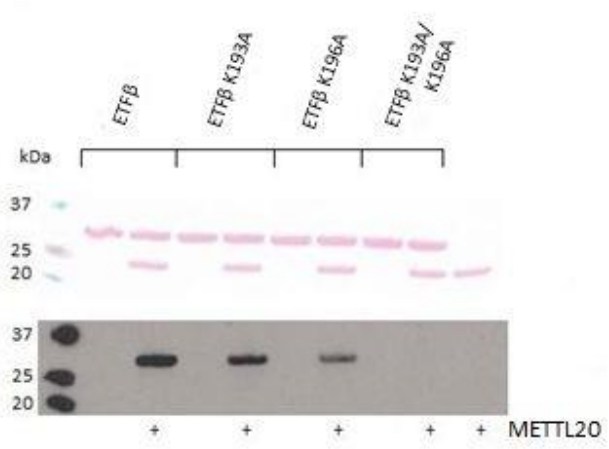

Figure 4.6 Methylation of recombinant ETFβ K193A, ETFβ K196A and ETFβ K193A/K196A by recombinant METTL20*. Reactions, containing proteins as indicated, were incubated with 3H-SAM (see Mat. and Meth.) and analyzed by SDS-PAGE followed by transfer of proteins to PVDF membrane. The membrane was stained with Ponceau S (upper panel) and exposed to X-ray film for fluorography (lower panel). The position of markers is shown on the left*

Based on these results, one may conclude that K193 and K196 are the residues that are being methylated, as the methylation band of ETFβ was only completely abolished when both these residues were mutated to alanine in the presence of SAM. Therefore, they represent true sites of methylation by METTL20 in vitro.

4.5 Generation of METTL20 knockout

In order to study the biological effects of methylation of identified substrates by METTL20, it was decided to generate a model organism containing a knockout for the METTL20 gene. *A. tumefaciens* was deemed a good choice as it contained the METTL20 orthologue, as well as

having other qualities making them advantageous to use including ease of handling and growth, a fully sequenced genome and ease of performing a gene knockout using the TargeTron system. The primers for retargeting the IBS, EBS1, EBS2 and δ sequences towards *A. tumefaciens* METTL20 were designed using the TargeTron primer design site, which resulted in a choice of multiple primer sets. The set chosen (see section 3.9) targeted the intron to insert between nucleotides 261 and 262 of the METTL20 gene. This corresponds to an insertion immediately after residue 87 of the peptide sequence, which is the last glycine of the METTL20 GXGXG sequence of motif I (see figure 1.5). In order to verify that pBL1 vector was present in *E. coli* DH5α containing the correctly re-targeted sequence, the PCR product of two colonies that tested positive in colony PCR for presence of pBL1 was gel extracted, purified and used as template for sequencing using fwd primer IBS and rev primer EBS1|δ. The sequencing results obtained using IBS primer as fwd allowed the checking of the retargeted EBS1|δ and EBS2 regions of the intron. Similarly, the sequencing results obtained using EBS1|δ primer as rev allowed the checking retargeted EBS2 and IBS regions of the intron. This way, the sequence of EBS2 could be read twice (in both directions), while the sequences of EBS1|δ and IBS were read once (figure 4.9).

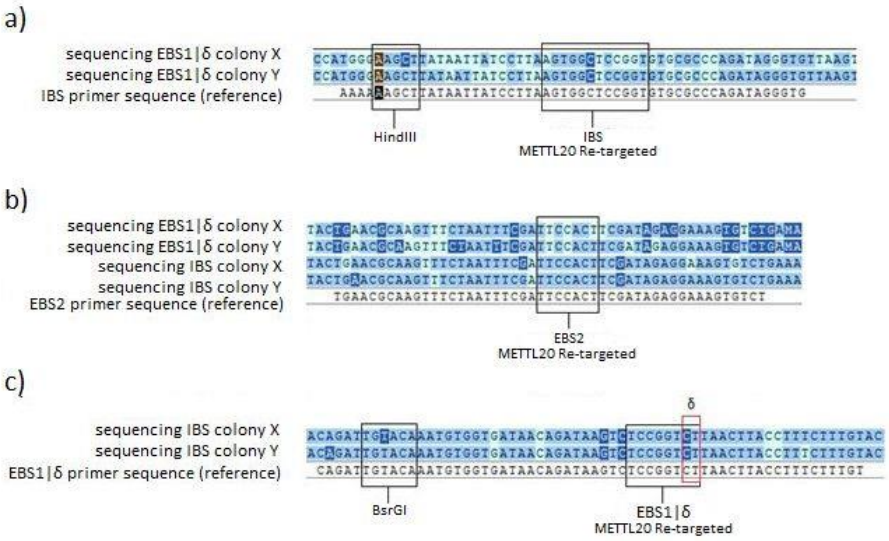

Figure 4.7 Sequencing analysis of pBL1 containing A.tumefaciens METTL20 re-targeted intron *a) IBS primer sequence as reference, with sequencing results using the EBS1|δ primer for two colonies. HindIII restriction site and region mutated to recognize retargeted EBS1 and EBS2. b) EBS2 primer sequence as reference, with sequencing results from a and b. Retargeted region indicated. c) EBS1|δ primer sequence as reference, with sequencing results using the IBS primer for two colonies. BsrGI restriction site, retargeted region and δ region indicated. Analysis performed in Sequencher.*

The colonies from which the sequenced plasmid originated were used to isolate the METTL20 re-targeted pBL1 plasmid. This plasmid was transformed into competent *A. tumefaciens* GV3101 pM90 cells. Transformants were tested by colony PCR using fwd primer IBS and rev primer EBS1|δ to check whether or not they contained METLL20-targeted pBL1 plasmid, as judged by the presence of a PCR product of ≈350bp (corresponding to the re-targeted region of the intron). Figure 4.10a shows that all seven colonies tested contained the pBL1 plasmid. Colonies from lanes 2 and 8 were further propagated and the intron's insertion into the METTL20 gene was induced by addition of m-toluic acid. After m-toluic acid induction, the cells were plated and screened in search of the METTL20 gene with inserted intron. The

screening was done by colony PCR using fwd primer IBS and rev primer EBS1|δ. Figure 4.10b shows that all tested colonies gave a PCR product of ≈1,500bp, indicative of the presence of the intron within the METTL20 gene. This corresponded well with the predicted size of the 650bp METTL20 gene with an added ≈900bp intron (Yao and Lambowitz, 2007).

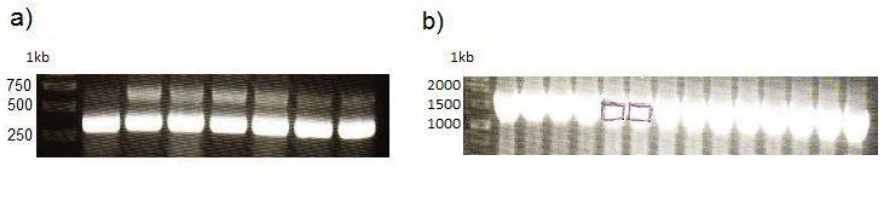

Figure 4.8 Colony PCR A.tumefaciens GV3101 pM90 a) Colony PCR of A.tumefaciens GV3101 pM90 transformed with pBL1 containing the intron retargeted towards the METTL20 gene using retargeting primers. b) Colony PCR of GV3101 pM90 colonies after induction with 5mM m-toluic acid using the METTL20 gene cloning primers. Samples run alongside GeneRuler 1kb Plus DNA ladder.

The PCR product from figure 4.9b lanes 6 and 7 was cut from the gel and purified in order to be used as template for sequencing with the METTL20 gene primers. This was done in order to verify the insertion by analyzing sequencing results as well as inspecting the site of insertion of the intron (figure 4.11a). As can be seen in figure 4.11b, the intron was inserted at the precise spot predicted by the TargeTron design site when primers were designed. The METTL20 gene was used as reference, and the sequencing results are identical up until the point of intron insertion. The 51 nucleotides following the site of insertion were translated using the ExPASy translation tool (appendix I). The reading frame in which the intron was inserted is shown in figure 4.10c, and shows the introduction of stop codons, causing the translation of a truncated protein.

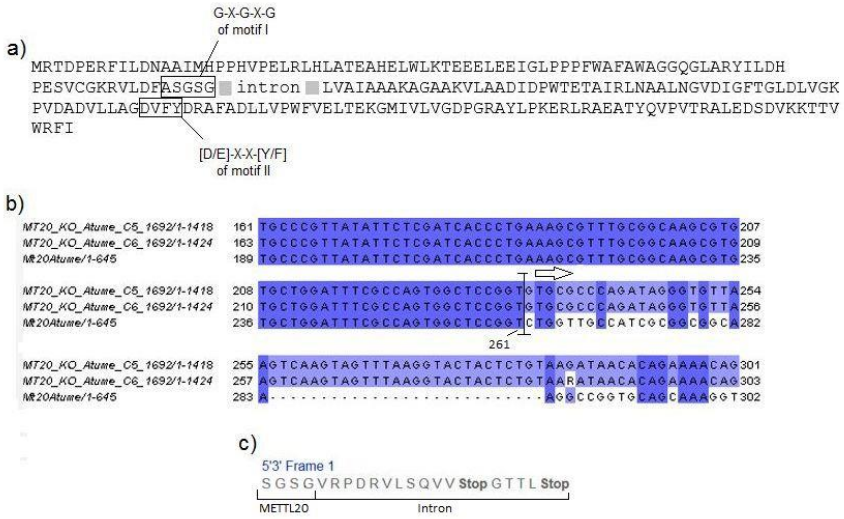

Figure 4.9 Sequencing METTL20 following intron insertion. *a) The peptide sequence of METTL20 including the intron site of insertion. The GXGXG sequence of motif I and [D/E]XX[Y/F] sequence of motif II are indicated. b) Sequencing results analyzed in Sequencher using the METTL20 gene sequence as reference (RefSeq: NP_001129335.1). Nucleotide 261 is indicated, from which the inserted intron sequence begins. c) Translation of the last 12 nucleotides of METTL20 and the first 51 nucleotides of the inserted intron sequence of sequencing results from b) using ExPASy., Stop codons indicated.*

The colonies that had their METTL20 gene with intron insertion sequenced (lanes 6 and 7 figure 4.10b) were used to cure the pBL1 plasmid, in order to have a KO strain that contained the

same genetic components as the WT. This was performed by growth without Tet antibiotic and plating. Twenty colonies were re-streaked on separate sectors on a plate containing Tet in order to test for viability. The colonies that were not viable on the Tet containing plate were again tested for presence of the METTL20 gene with inserted intron by colony PCR using fwd primer IBS and rev primer EBS1|δ. The colony PCR was extended to include GV3101 pM90 WT, METTL20 KO uninduced, METTL20 KO induced and METTL20 KO pBL1 cured strains (figure 4.12). A final colony that contained the intron in the METTL20 gene and had lost the pBL1 plasmid was used as the final GV3101 pM90 METTL20 KO strain.

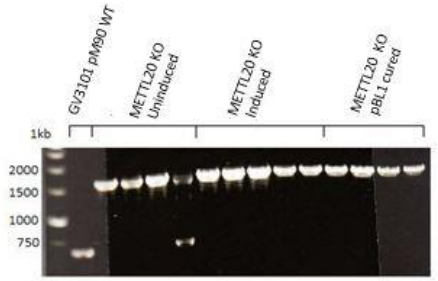

Figure 4.10 Colony PCR A.tumefaciens GV3101 pM90 METTL20 KO. *(from left) A.tumefaciens GV3101 pM90 WT strain, 4 GV3101 pM90 METTL20 KO strains containing pBL1 plasmid with intron but uninduced, 5 GV3101 pM90 METTL20 KO strains containing pBL1 plasmid with intron after induction, and 4 GV3101 pM90 METTL20 KO strains after induction and pBL1 curing.*

As can be seen in figure 4.12, induction had occurred prior to induction. Only one colony gave a PCR product of 650bp corresponding to the METTL20 gene, but even this colony had some PCR product of ≈1,500bp corresponding to intron insertion into the METTL20 gene.

Based on the results, the introduction of the intron to the METTL20 gene of *A. tumefaciens* GV3101 pM90 was successful, as was the curing of the pBL1 plasmid. This strain of METTL20 KO could now be used in further studies using the GV3101 pM90 WT as reference, as the WT and METTL20 strains differed only in the METTL20 gene and were otherwise genetically identical in regards to genome and plasmids.

4.6 Growth comparisons of *A. tumefaciens GV3101 pM90 WT and METTL20 KO*

In order to determine a biological phenotype for the METTL20 KO strain of GV3101 pM90, a series of experiments were performed to determine if the growth rate of the two strains differed under a certain condition. All experiments in which growth on sole carbon sources or under osmotic stress were tested are shown in appendix II. First we tested whether the METTL20 KO would differ from the WT when grown in YEB or M9 medium containing glucose as the sole carbon source, supplemented with Rif and Gent. Growth rate was measured using OD600 over a period of time. For growth in glucose, there was no significant difference in growth rate between the WT and METTL20 KO strains. In YEB medium, growth rates were extremely variable as in some cases the WT cells outperformed METTL20 KO cells in regards to growth rate, whereas other times the results showed the opposite. This indicated that YEB medium was not a good medium for assessing growth rates.

As the METTL20 substrate ETFβ is involved in a number of metabolic pathways, experiments were performed in which these metabolic pathways would be used for growth by addition of carbon sources specific to each pathway. M9 medium was used with Rif and Gent. ETFβ and its interaction with MCAD was tested using medium-chain fatty acid octonoate as the sole carbon-source. For IVD, leucine was used as the sole carbon source. For GCD, lysine was used as the sole carbon source. Even over an extensive period of time, no visible growth was observed for cultures of WT and METTL20 KO cells grown in M9 containing octonoate (figure 4.13d), lysine or leucine as sole carbon sources. An experiment was run in which the strains were grown in M9 containing leucine, lysine and glucose. This was done in order to see if any differences in growth were observable when growing on amino acids with a small amount of glucose present. There was a very low amount of growth, and no differences in growth rate were observed (figure 4.13e). For DMGD, choline and betaine were used as sole carbon sources. Betaine is a product of choline degradation, and ultimately are part of the same pathway. For SARD, sarcosine was used as the sole carbon source. Growth using betaine, choline and sarcosine as sole carbon sources did not appear to yield large differences in growth rates (figure 4.14a-c). In figure 4.14b, in which cells were grown with choline as sole carbon source, there appears to be a difference in growth rates between the WT and METTL20 cells. However, when the other experiments with choline as sole carbon source shown in appendix II are taken into account, the difference shown here is likely due to differences in initial amounts of cells added at the start of the culture.

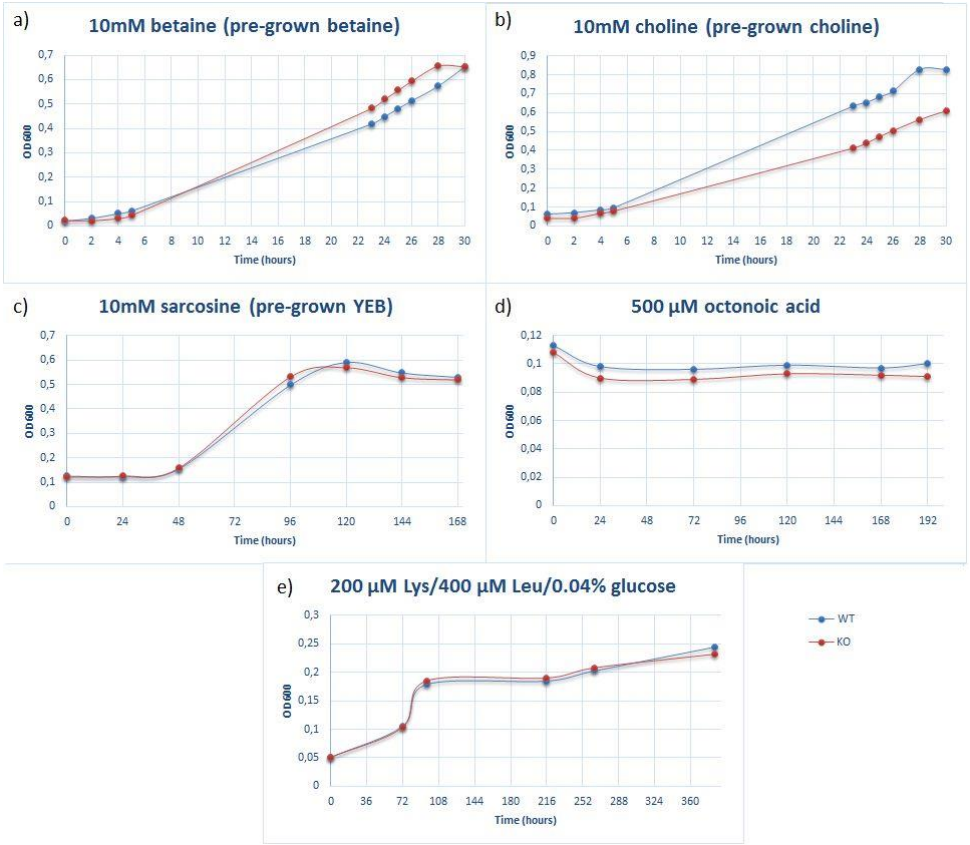

Figure 4.11 Growth comparisons of A.tumefaciens GV3101 pM90 WT and METTL20 KO strains utilizing defined carbon sources *Growth of the strains in M9 medium supplemented with a) 10mM betaine, b) 10mM choline, c) 10mM sarcosine, d) 500µM octonoic acid (octonoate), e) 200µM lysine/400µM leucine/0.04%glucose as carbon sources. Growth rates as a function of OD600 versus time.*

As no growth was observed when octonoate, lysine and leucine were the sole carbon sources, it was desired to inspect if there was a difference between the WT and KO strain in regards to viability. 100µL was taken from WT and KO medium containing these carbon sources and plated on M9 plates containing antibiotics and glucose. The plates were incubated at 28°C overnight. As can be seen in figure 4.14, differences in viability could not be detected on the count of both the WT and METTL20 KO strains growing superbly once introduced to media with glucose as the carbon source, covering the entire area of the plate on which the cells were applied.

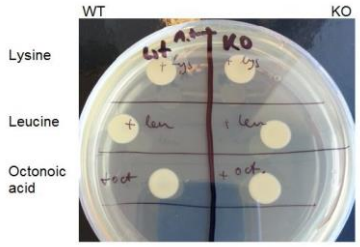

Figure 4.12 Determination of viability for cells grown in lysine, leucine and octonoic acid. *Plate with M9 medium containing 22.2mM glucose, on which 100µL of A.tumefaciens GV3101 pM90 WT and METTL20 KO containing medium growing with lysine, leucine or octonoic acid (octonoate) as sole carbon sources were plated. Plates were incubated overnight at 28°C.*

Growth under osmotic stress was achieved by addition of NaCl in high amounts to the growth medium. Several concentrations were tested, however 0.3M NaCl was assumed to be an appropriate level. At this amount of NaCl, cells were clearly stressed compared to growth in medium with the same carbon sources but without NaCl, however growth was not completely inhibited. Carbon sources used during osmotic stress were 10mM betaine, 10mM choline and 10mM sarcosine. As can be seen in figure 4.16, there appeared to be a small difference in the growth rate for the strains when grown under osmotic stress utilizing betaine and choline as sole carbon sources. However, once again the results found in appendix II would often yield more similar growth rates and so the difference shown here is likely due to differences in initial amounts of cells added at the start of the culture.

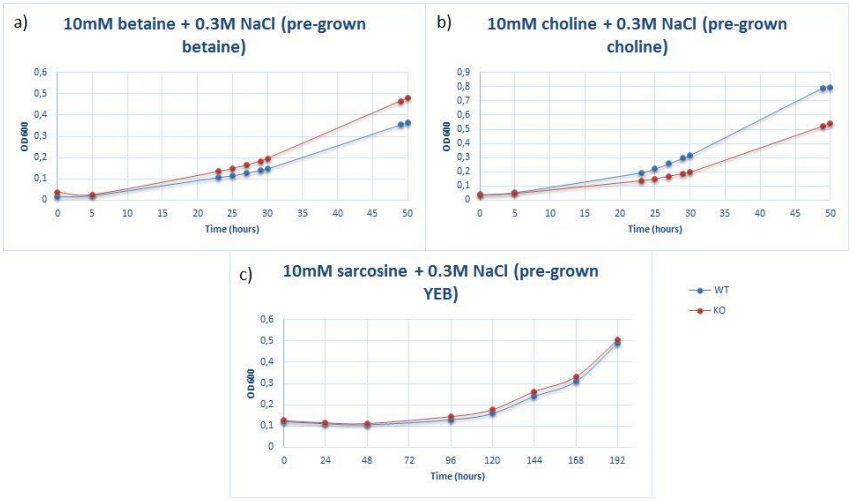

Figure 4.13 Growth comparison of A.tumefaciens GV3101 pM90 WT and METTL20 KO strains under osmotic stress. *Cells grown under osmotic stress by addition of 0.3M NaCl M9 medium supplemented with a) 10mM betaine, b) 10mM choline and c) 10mM sarcosine as sole carbon sources. Growth rates as a function of OD600 versus time.*

Oxidative stress was also tested, using both YEB and M9 medium containing glucose as growth medium, and H_2O_2 to stress the cells. The cells were stressed for 15 minutes with 2mM H_2O_2 in the medium prior to resuspension in new growth medium supplemented with glucose. As can be seen in figure 4.17, the growth rate for the strains appeared to be near identical when grown after a 15 minute H_2O_2 stressing period.

Figure 4.14 Growth comparison of A.tumefaciens GV3101 pM90 WT and METTL20 KO strains when grown under oxidative stress. *Cells stress by 15 minutes growth in the presence of 2mM H_2O_2 in M9 medium supplemented with glucose. Growth rates as a function of OD600 versus time.*

Anaerobic growth of the WT and KO strains on YEB plates was not achieved, as none of the dilutions plated gave rise to any colonies. Upon removal from the airtight Oxoid Anaerogen container, many colonies grew in all dilutions overnight in numbers that could not be counted.

The most promising results came from testing viability of the strains under heat-shock stress. The first experiment was performed by the strains being plated on YEB plates and grown overnight at 37°C in order to stress the cells by growth at higher than normal temperatures. Once the cells were removed from 37°C, they were incubated at RT overnight. Colonies formed can be seen in figure 4.18, and show how the WT strain appeared to be more resistant towards heat stress.

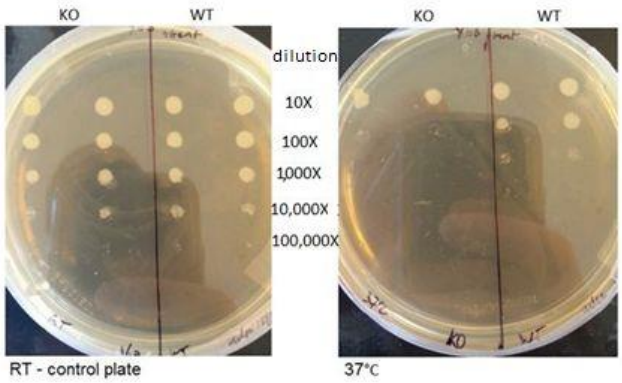

Figure 4.15 Overnight heat shocking of A.tumefaciens GV3101 pM90 WT and METTL20 KO strains*. Heat-shock of the cells performed on YEB plates grown at 37°C overnight and a control plate grown overnight at RT. Plating was performed in dilutions ranging from 10X to 100,000X.*

The second form of heat-shock experiment was performed by growing identical amounts of cells and exposing them to 50° for 5, 10, 15 and 20 minutes and plating them in dilutions on

YEB plates. The plates were incubated at 28°C. As can be seen in figure 4.19, it was observed that yet again, there appeared to be a higher survival rate of WT cells in comparison to METTL20 KO cells after heat shocking.

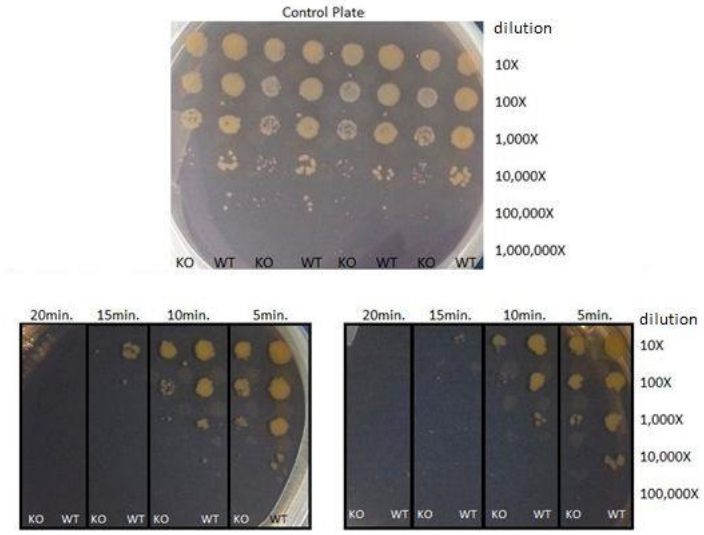

Figure 4.16 Heat-shocking of A.tumefaciens G3101 pM90 WT and METTL20 KO strains at 50°C for varying amounts of time. *Cells of both strains were grown for 5, 10, 15 and 20 minutes at 50°C. The heat shocking was performed in duplicate. Dilutions were made in the range of 10X-1,000,000X. Experimental control was cells of WT and METTL20 KO cells plated prior to heat shocking in the same dilution range as the heat-shocked cells. Plates grown at 28°C after heat shocking.*

The final heat-shock experiment was performed somewhat differently than previous experiments. Heat shocking was performed at 50°C for 15 minutes using cultures measured to OD600 0.1. The cells were diluted in series and selected dilutions were plated on YEB plates, after which the plates were incubated at room temperature. The control plates for the WT and METTL20 strains were done forming their colonies after 48 hours incubation time. In figure 4.21, it appears that the control plates contained relatively equal amounts of colonies, which was confirmed by counting colonies. After heat-shocking however, whereas the WT cells formed most all of its colonies within 48 hours as was the case for the controls, the METTL20 KO cells needed an additional 48 hours for all colonies to be formed. After 96 hours of incubation times, all colonies appeared to have been formed. After 96 hours, visually the plates containing the WT cells after heat stressing appeared to form far more colonies than the METTL20 cells in the 10X dilutions. The same appeared to be true in the 100X dilutions, although the difference did not appear to be as apparent as for the 10X. Counting the colonies confirmed the presence of more colonies for the WT strain than the METTL20 KO strain in the 100X dilution. Interestingly, despite the controls invariably giving rise to more colonies of the METTL20 KO strain in comparison to the WT strain, after heat shocking the WT strain appeared to give rise to more colonies than the METTL20 KO strain.

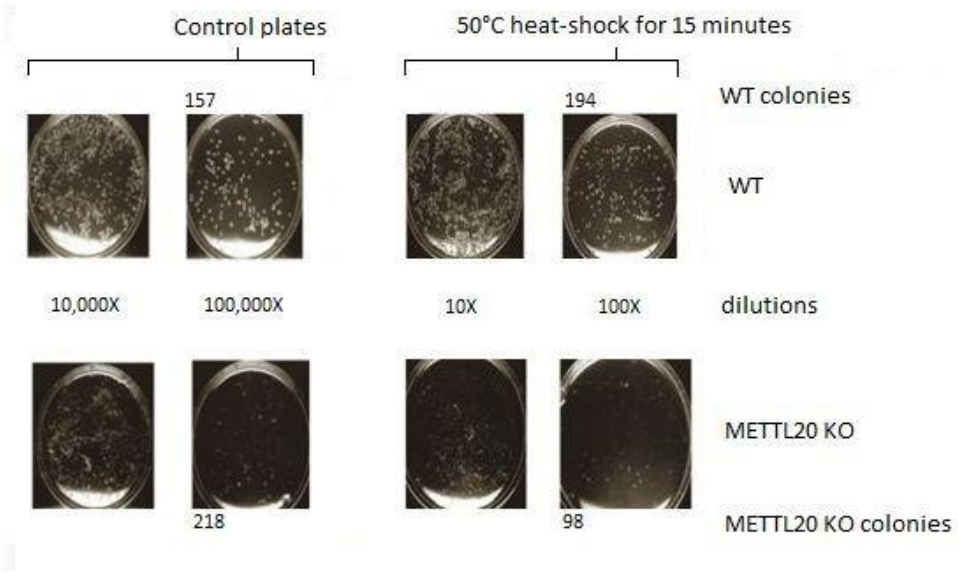

Figure 4.17 Growth comparison of A.tumefaciens GV3101 pM90 WT and METTL20 KO strains after 15 minutes heat shocking at 50°C. *The controls were plated by making dilutions of the WT and METTL20 strains prior to heat shocking of 10,000X and 100,000X. After heat shocking of the cells, 10X and 100X dilutions were made and plated. Plates were incubated at RT for a total of 96 hours before counting the colonies.*

Based on these results, it would appear that the phenotype for the METTL20 KO in some involves heat shocking, although it is unclear if the phenotype is reduced viability at elevated temperatures, reduced growth rate or both.

5. Discussion

5.1 Methyltransferase function of METTl20

The role of METTL20 was inferred using bioinformatics, which classified this enzyme as belonging to Family 16 MTases, together with nine other enzymes. They contained the conserved motifs typical for 7BS MTases, with an added motif denoted the (D/E)XX(Y/F) (Kernstock et al., 2012). Bioinformatics performed in regards to the structure of METTL20 was presented in the introduction of this thesis, shown in figure 5 of section 1.1.2. The figure contains a short but detailed description as to how the figure was made, and from the figure it can be confirmed that METTL20 contains all the conserved motifs belonging to 7BS MTases of Fam16. The conserved common 7BS core structures were also found for METTL20. A group had found METTL20 to be pre-dominantly localized to cytoplasmic granular foci, (Cloutier et al., 2013). Identification of ETFβ as the substrate for *A. tumefaciens* METTL20, as well as confirmation of ETFβ1 as a substrate of the human METTL20 leans away from granular foci and more towards mitochondrial localization as ETFβ1 is found in the mitochondrias of humans. This observation matches the findings that METTL20 localizes to the mitochondria found by microscopy by Malecki et al, as mentioned in section 1.1.2. The alignment in figure 5.1 shows how the human METTL20 contains an N-terminal extension not found on the bacterial enzyme. This may reflect the need for sub-cellular localization signalling. When the N-terminal extension of the human enzyme was analyzed by the Yloc sub-cellular localization predictor, the peptide sequence was predicted to be targeted to the mitochondria with 87.8% probability (Briesemeister et al., 2010a, 2010b). METTL20 does not appear to need any co-enzymes or additional sources of energy to carry out its enzymatic activity, as MTase activity was possible so long as METTL20 was incubated with a substrate and SAM, a metabolically activated methyl donor. It is also apparent that METTL20 contains a site on which it automethylates, as multiple fluorographies have resulted in bands at METTL20s location in the membrane.

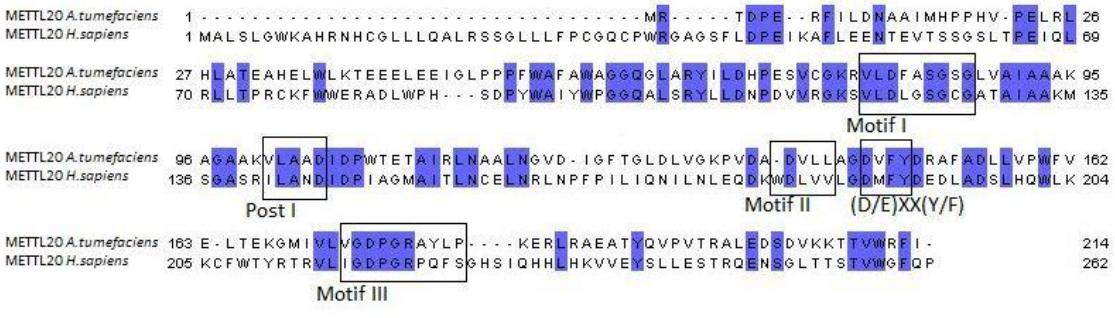

Figure 5.1 Sequence alignment of A.tumefaciens and H.sapiens METTL20. *Sequence alignment METTL20 of A.tumefaciens (RefSeq:AAK88369.1) and H.sapiens (RefSeq:NP_001129335.1) performed using MUSCLE (Edgar, 2004).*

5.2 Substrates

RpL7/L12 was identified as a true substrate for *A. tumefaciens* METTL20, identified by MS and validated by fluorography in this thesis. The human mRpL12 however, is not methylated by either the human nor bacterial METTL20 (Malecki et al., unpublished). The site of methylation, K86, lies on the C-terminal region of RpL7/L12. The C-terminal RpL7/L12 region is known to carry the function of recruiting translational factors, as well as stimulation of GTPase activity as discussed in the introduction. The residues that appear to be involved in the interactions with the translational factors have been characterized. The residues are V66, A67, V68, K70, G79, L80 and E82 (Helgstrand et al., 2007). The residues involved in the interactions are shown in figure 5.1.

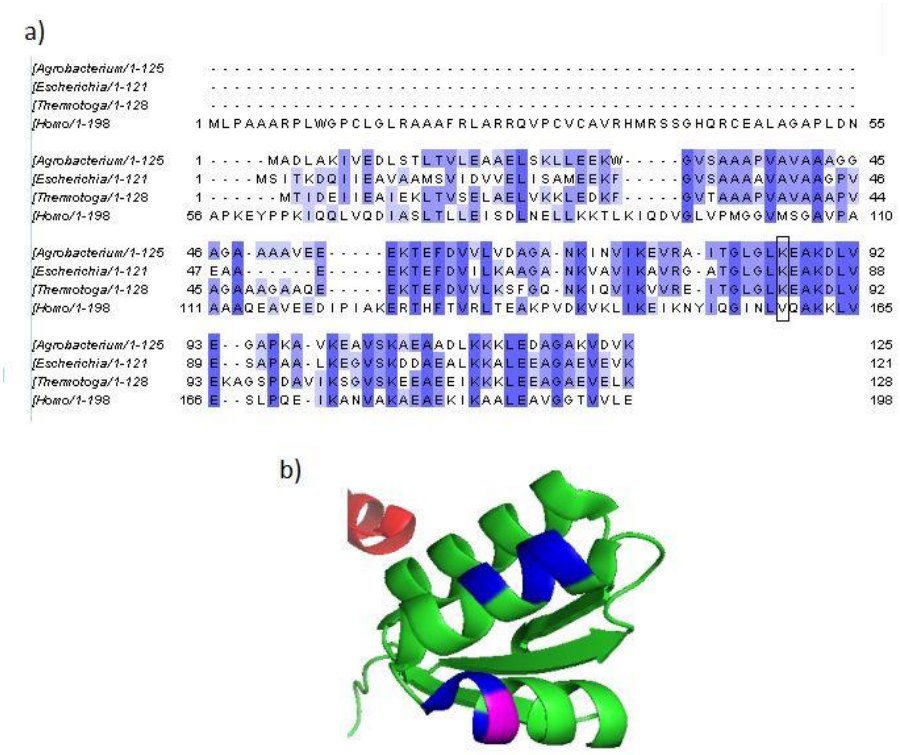

Figure 5.2 Sequence alignment and structure of C-terminal RpL7/L12 *a) sequence alignment of A.tumefaciens RpL7/L12 (RefSeq: NP_354932.1), E.coli RpL7/L12 (RefSeq: WP_001498596.1), Thermotoga maritime (RefSeq: WP_004081509.1) and H.sapiens mRpL12 (RefSeq: NP_002940.2) performed using MUSCLE (Edgar, 2004). The residues corresponding to K86 of A.tumefaciens RpL7/L12 boxed in. b) C-terminal region of E.coli RpL7/L12 (PDB:1RQU) modelled in PyMol (Schrodinger, 2010). Key residues involved in interaction with translational factors in blue, K82 of E.coli corresponding to K86 of A.tumefaciens in magenta.*

The sequence alignment in figure 5.1a shows how the residue in *H. sapiens* mRpL12 corresponding to K86 of *A. tumefaciens* RpL7/L12 has not been conserved. This may offer an explanation as to why the human METTL20 does not methylate mRpL12. The structure of *E.coli* RpL7/L12 shown in figure 5.1b shows how the residue corresponding to K86 of *A. tumefaciens* is located between two residues involved in interactions with translational factors. This may indicate that methylation of this site potentially in some way is related to interactions involving RpL7/L12 and translational factors. The lysine of *E. coli* RpL7/L12 corresponding to K86 of *A. tumefaciens* has been observed to have its methylation state altered when exposed

to reduced temperatures, however the responsible MTase is yet to be discovered (Nesterchuk et al., 2011).

The second substrate characterized in this thesis that is methylated by METTL20 is ETFβ, with methylation sites K193 and K196. These residues correspond to K200 and K203 of *H. sapiens* ETFβ1. K200 in *H. sapiens* is annotated in Phosphosite Plus (appendix I) to be methylated, however K203 is not annotated as being methylated. The *A. tumefaciens* METTL20 was capable of methylating *H. sapiens* ETFβ1, which is explained by the fact that human METTL20 recognizes ETFβ1 as its substrate (Malecki et al., unpublished). As the site of methylation is very similar between ETFβ and ETFβ1, the bacterial METTL20 appears to recognize the human substrate. The two methylation sites are likely located near the interaction site between ETF and primary dehydrogenases, as can be seen in figure 5.3b, in which the structure of *H. sapiens* ETF interacting with MCAD has been solved (Toogood et al., 2004).

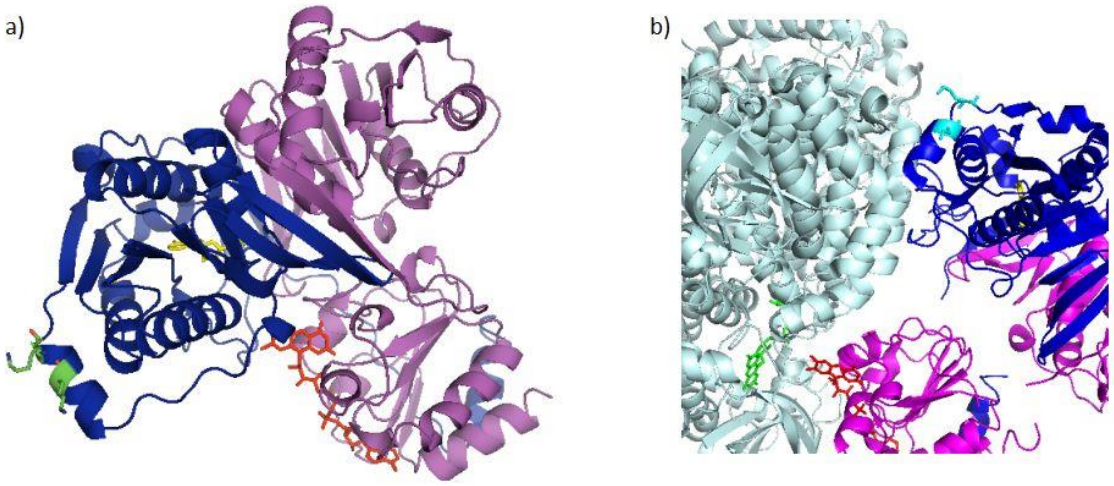

Figure 5.3 Solved structure of H.sapiens ETF interacting with MCAD *a) ETF alpha subunit in magenta and beta subunit in blue, FAD in red, and AMP in yellow. K200 and K203 indicated by green. b) different angle of the ETF with alpha subunit in magenta, beta subunit in blue, FAD in red, AMP in yellow and lysine residues K200 and K203 in light blue.. ETF interacting with MCAD shown in grey, with MCAD FAD co-factor shown in green. PDB:2A1T.*

K200 and K203 of ETF are located on an alpha-helix that is situated out towards the solvent (figure5.3a). The METTL20 targeted lysines are light blue on the blue ETFβ1 chain in figure 5.3b, and appear to be located on and just proximal to an alpha-helix that is involved in interactions between ETF and MCAD. In this structure, the FAD of ETF (red sticks) is brought close to FAD on MCAD (green sticks), and is involved in the transition of electrons from the primary dehydrogenase to ETF. As the residues methylated by METTL20 lie in close proximity to the region of ETF interacting with MCAD in this solved structure, it is tempting to assume that methylation of these sites in some way are involved with interactions of ETF with the dehydrogenases.

5.3 Biological function

As previously mentioned, the human METTL20 does not methylate mRpL12, but does methylate ETFβ1. Therefore, the majority of experiments designed to elucidate the biological function of METTL20 were directed at the role of ETFβ methylation.

The majority of experiments performed did not show any major differences between *A. tumefaciens* GV3101 pM90 WT and METTL20 strains. This does not mean that the role of METTL20 methylation does not lie within one of the tested conditions, as it may be that the experiments may not have been sensitive enough to detect the differences. A better method of detecting differences between the WT and METTL20 KO strains when grown on different carbon sources for example, could be to perform an enzymatic assay in order to detect ETF activity when in reaction with dehydrogenases and a terminal electron acceptor. If performed using both ETF containing ETFβ from the WT strain and METTL20 KO strain, a difference might be observed. Due to the biological role of ETFβ methylation by METTL20 being completely unknown, the only clues was the substrate itself, and which tasks it performs in vivo. The identification of the biological role was not simplified by the fact that ETF interacts with a number of dehydrogenases. Furthermore, the role could be some form of regulation, or play a role in recognition by an interaction partner, increasing the parameters that may need to be tested. The experiments performed for this thesis were performed in a manner to cover a broad ground, including various stress conditions as well as testing the metabolic pathways ETF is involved in. It could also be that the role of methylation by METTL20 lies within a pathway not yet tested, such as some additional fatty-acid dehydrogenase such as the long-chain fatty acid dehydrogenase (LCAD). Heat-shock does appear to produce a phenotype in the KO strain, and should be tested further. It was not determined during this thesis if this was a true phenotype due to results not being completely convincing. Nevertheless, it is clear that there is potential in this phenotype as each experiment performed generated a difference between the two strains, with the WT strain appearing to be more resistant towards heat-shock than the METTL20 KO. It has also not been determined whether the potential phenotype is caused by loss of RpL7/L12 K86 methylation, or ETFβ K193 and K196 methylation. If the heat-shock sensitivity was the true METTL20 phenotype, the hypo-methylated substrate responsible could be determined. This could be determined by complementing the METTL20 KO strain with *H. sapiens* METTL20, as it methylates ETFβ but not RpL7/L12. If the phenotype is rescued, it would indicate that hypo-methylation of ETFβ was responsible for the METTL20 phenotype. If the phenotype is not rescued, hypo-methylation of RpL7/L12 would be responsible for the METTL20 phenotype.

5.4 Conclusion

A. tumefaciens and *H. sapiens* METTL20 are lysine specific MTases, targeting non-histone proteins. The bacterial enzyme is responsible for the methylation of K86 of RpL7/L12 as well as K193 and K196 of ETFβ. The human enzyme methylates only ETFβ1, at residues K200 and K203 (Malecki et al., unpublished). The biological role of METTL20 has not been characterized yet, however in this thesis a potential phenotype has been uncovered for the *A. tumefaciens* METTL20 KO strain created. The KO strain appears to be more sensitive towards heat shocking, although it was not found whether it was because of reduced viability of the

METTL20 KO cells or if the cells merely grew at a reduced rate. Further studies can be performed utilizing the METTL20 KO strain generated in order to uncover the biological role.

6. Future Perspectives

The METTL20 KO strain would need to be used in further studies involving heat-shock stress, in order to confirm that sensitivity towards heat-shock is the true METTL20 KO phenotype.

If the heat-shock phenotype is not the true phenotype, more detailed studies of ETFβ and its interactions with primary dehydrogenases should be performed. Enzymatic assays should be run in which either hypo-methylated ETFβ (from METTL20 KO cells) or WT methylation state ETFβ is run in a reaction with the dehydrogenases ETF interacts with in vivo. This should be performed using heterodimeric ETF, and the reaction would need substrate specific for the dehydrogenase being tested. The reaction would also include a detectable terminal electron acceptor, such as a redox indicator, which will have different colours depending on its oxidation state. This would allow for measurements to be taken of the rate at which ETF reduces the indicator. The assays would give more accurate and sensitive results, which when compared may reveal a difference in ETF redox rates between the WT and METTL20 KO ETFβ.

As previously stated, with two substrates targeted by *A. tumefaciens* METTL20, it is necessary to identify which substrate is responsible for any potential phenotypes. This would need to be done by introducing the *H. sapiens* METTL20 into the METTL20 KO strain once a phenotype is identified, which will only methylate ETFβ. In this manner, if the phenotype is rescued, ETFβ hypo-methylation due to lack of METTL20 is the cause of the phenotype.

It may also be of interest to identify the MTase responsible for methylation of *E. coli* RpL7/L12 on K82, as there is no orthologue of METTL20 identified in *E. coli*. There may be some form of similarity between this MTase and METTL20, as it shares a similar function. This might shed some light on the evolution of METTL20.

References

Alberts, B., Johnson, A., Lewis, J., Raff, M., Roberts, K., and Walter, P. (2007). The RNA Message is Decoded in Ribosomes. In Molecular Biology of the Cell, (Garland Science), p. 1392.

Blatny, J.M., Brautaset, T., Winther-Larsen, H.C., Karunakaran, P., and Valla, S. (1997). Improved Broad-Host-Range RK2 Vectors Useful for High and Low Regulated Gene Expression Levels in Gram-Negative Bacteria. Plasmid *38*, 35–51.

Blom, H.J., and Smulders, Y. (2011). Overview of homocysteine and folate metabolism. With special references to cardiovascular disease and neural tube defects. J. Inherit. Metab. Dis. *34*, 75–81.

Briesemeister, S., Rahnenführer, J., and Kohlbacher, O. (2010a). YLoc—an interpretable web server for predicting subcellular localization. Nucleic Acids Res. *38*, W497–W502.

Briesemeister, S., Rahnenführer, J., and Kohlbacher, O. (2010b). Going from where to why—interpretable prediction of protein subcellular localization. Bioinformatics *26*, 1232–1238.

Clarke, S.G. (2013). Protein methylation at the surface and buried deep: thinking outside the histone box. Trends Biochem. Sci. *38*, 243–252.

Cloutier, P., Lavallée-Adam, M., Faubert, D., Blanchette, M., and Coulombe, B. (2013). A Newly Uncovered Group of Distantly Related Lysine Methyltransferases Preferentially Interact with Molecular Chaperones to Regulate Their Activity. PLoS Genet *9*, e1003210.

Cousineau, B., Smith, D., Lawrence-Cavanagh, S., Mueller, J.E., Yang, J., Mills, D., Manias, D., Dunny, G., Lambowitz, A.M., and Belfort, M. (1998). Retrohoming of a Bacterial Group II Intron: Mobility via Complete Reverse Splicing, Independent of Homologous DNA Recombination. Cell *94*, 451–462.

Diaconu, M., Kothe, U., Schlünzen, F., Fischer, N., Harms, J.M., Tonevitsky, A.G., Stark, H., Rodnina, M.V., and Wahl, M.C. (2005). Structural Basis for the Function of the Ribosomal L7/12 Stalk in Factor Binding and GTPase Activation. Cell *121*, 991–1004.

Edgar, R.C. (2004). MUSCLE: multiple sequence alignment with high accuracy and high throughput. Nucleic Acids Res. *32*, 1792–1797.

Finkelstein, J.D. (1998). The metabolism of homocysteine: pathways and regulation. Eur. J. Pediatr. *157*, S40–S44.

Frerman, F.E., and Goodman, S.I. (1985). Deficiency of electron transfer flavoprotein or electron transfer flavoprotein:ubiquinone oxidoreductase in glutaric acidemia type II fibroblasts. Proc. Natl. Acad. Sci. *82*, 4517–4520.

Helgstrand, M., Mandava, C.S., Mulder, F.A.A., Liljas, A., Sanyal, S., and Akke, M. (2007). The Ribosomal Stalk Binds to Translation Factors IF2, EF-Tu, EF-G and RF3 via a Conserved Region of the L12 C-terminal Domain. J. Mol. Biol. *365*, 468–479.

Huang, C., Mandava, C.S., and Sanyal, S. (2010). The Ribosomal Stalk Plays a Key Role in IF2-Mediated Association of the Ribosomal Subunits. J. Mol. Biol. *399*, 145–153.

Jakobsson, M.E., Moen, A., Bousset, L., Egge-Jacobsen, W., Kernstock, S., Melki, R., and Falnes, P.Ø. (2013). Identification and Characterization of a Novel Human Methyltransferase Modulating Hsp70 Protein Function through Lysine Methylation. J. Biol. Chem. *288*, 27752–27763.

Katz, J.E., Dlakić, M., and Clarke, S. (2003). Automated Identification of Putative Methyltransferases from Genomic Open Reading Frames. Mol. Cell. Proteomics *2*, 525–540.

Kernstock, S., Davydova, E., Jakobsson, M., Moen, A., Pettersen, S., Mælandsmo, G.M., Egge-Jacobsen, W., and Falnes, P.Ø. (2012). Lysine methylation of VCP by a member of a novel human protein methyltransferase family. Nat. Commun. *3*, 1038.

Kothe, U., Wieden, H.-J., Mohr, D., and Rodnina, M.V. (2004). Interaction of Helix D of Elongation Factor Tu with Helices 4 and 5 of Protein L7/12 on the Ribosome. J. Mol. Biol. *336*, 1011–1021.

Lambowitz, A.M., and Zimmerly, S. (2004). Mobile Group II Introns. Annu. Rev. Genet. *38*, 1–35.

Li, W., Guo, G., and Zheng, G. (2000). Agrobacterium-mediated transformation: state of the art and future prospect. Chin. Sci. Bull. *45*, 1537–1546.

Lin, K., Simossis, V.A., Taylor, W.R., and Heringa, J. (2005). A simple and fast secondary structure prediction method using hidden neural networks. Bioinformatics *21*, 152–159.

Luís, P.B.M., Ruiter, J.P.N., IJlst, L., Almeida, I.T. de, Duran, M., Mohsen, A.-W., Vockley, J., Wanders, R.J.A., and Silva, M.F.B. (2011). Role of Isovaleryl-CoA Dehydrogenase and Short Branched-Chain Acyl-CoA Dehydrogenase in the Metabolism of Valproic Acid: Implications for the Branched-Chain Amino Acid Oxidation Pathway. Drug Metab. Dispos. *39*, 1155–1160.

Magnani, R., Dirk, L.M.A., Trievel, R.C., and Houtz, R.L. (2010). Calmodulin methyltransferase is an evolutionarily conserved enzyme that trimethylates Lys-115 in calmodulin. Nat. Commun. *1*, 43.

De Mello Serrano, G.C., e Silva Figueira, T.R., Kiyota, E., Zanata, N., and Arruda, P. (2012). Lysine degradation through the saccharopine pathway in bacteria: LKR and SDH in bacteria and its relationship to the plant and animal enzymes. FEBS Lett. *586*, 905–911.

Metallo, C.M. (2012). Expanding the Reach of Cancer Metabolomics. Cancer Prev. Res. (Phila. Pa.) *5*, 1337–1340.

Misono, H., and Nagasaki, S. (1982). Occurrence of l-Lysine ?-Dehydrogenase in Agrobacterium tumefaciens. J. Bacteriol. *150*, 398–401.

Mohr, D., Wintermeyer, W., and Rodnina, M.V. (2002). GTPase Activation of Elongation Factors Tu and G on the Ribosome†. Biochemistry (Mosc.) *41*, 12520–12528.

Nesterchuk, M.V., Sergiev, P.V., and Dontsova, O.A. (2011). Posttranslational Modifications of Ribosomal Proteins in Escherichia coli. Acta Naturae *3*, 22–33.

Patananan, A.N., Palmer, J.M., Garvey, G.S., Keller, N.P., and Clarke, S.G. (2013). A Novel Automethylation Reaction in the Aspergillus nidulans LaeA Protein Generates S-Methylmethionine. J. Biol. Chem. *288*, 14032–14045.

Petrossian, T.C., and Clarke, S.G. (2009). Multiple Motif Scanning to Identify Methyltransferases from the Yeast Proteome. Mol. Cell. Proteomics MCP *8*, 1516–1526.

Ragsdale, S.W. (2008). Catalysis of methyl group transfers involving tetrahydrofolate and B(12). Vitam. Horm. *79*, 293–324.

Schrodinger, L. (2010). The PyMOL Molecular Graphics System.

Schubert, H.L., Blumenthal, R.M., and Cheng, X. (2003). Many paths to methyltransfer: a chronicle of convergence. Trends Biochem. Sci. *28*, 329–335.

Simkovic, M., and Frerman, F.E. (2004). Alternative quinone substrates and inhibitors of human electron-transfer flavoprotein-ubiquinone oxidoreductase. Biochem. J. *378*, 633–640.

Stelzl, U., Connell, S., Nierhaus, K.H., and Wittmann-Liebold, B. (2001). Ribosomal Proteins: Role in Ribosomal Functions. In eLS, (John Wiley & Sons, Ltd),.

Thorpe, C., and Kim, J.J. (1995). Structure and mechanism of action of the acyl-CoA dehydrogenases. FASEB J. *9*, 718–725.

Toogood, H.S., Thiel, A. van, Basran, J., Sutcliffe, M.J., Scrutton, N.S., and Leys, D. (2004). Extensive Domain Motion and Electron Transfer in the Human Electron Transferring Flavoprotein·Medium Chain Acyl-CoA Dehydrogenase Complex. J. Biol. Chem. *279*, 32904–32912.

Toogood, H.S., Leys, D., and Scrutton, N.S. (2007). Dynamics driving function − new insights from electron transferring flavoproteins and partner complexes. FEBS J. *274*, 5481–5504.

Warner, J.R., and McIntosh, K.B. (2009). How Common Are Extraribosomal Functions of Ribosomal Proteins? Mol. Cell *34*, 3–11.

Wittwer, A.J., and Wagner, C. (1981). Identification of the folate-binding proteins of rat liver mitochondria as dimethylglycine dehydrogenase and sarcosine dehydrogenase. Purification and folate-binding characteristics. J. Biol. Chem. *256*, 4102–4108.

Yao, J., and Lambowitz, A.M. (2007). Gene Targeting in Gram-Negative Bacteria by Use of a Mobile Group II Intron ("Targetron") Expressed from a Broad-Host-Range Vector. Appl. Environ. Microbiol. *73*, 2735–2743.

Appendix I

World wide web references.

1. PrimerX - http://www.bioinformatics.org/primerx/index.htm
2. TargeTron design site - http://www.sigma-genosys.com/targetron/
3. Sequencher - http://www.genecodes.com/
4. ExPASy translation tool - http://web.expasy.org/translate/
5. Phosphosite Plus - http://www.phosphosite.org/homeAction.do

Appendix II

OD600 measurements taken of *A.tumefaciens* GV3101 pM90 WT and KO strains grown in different growth conditions, in either YEB medium or M9 medium.

Strain	Media	C-source/condition	Start Date	OD	Date	OD	Date	OD	Date	OD	Date	OD	Date	OD	Date	OD	Date	OD
WT	M9	0.4% glucose	15.09.2013	0,05	16.09.2013	0,239	17.09.2013	0,39	18.09.2013	0,377	19.09.2013	0,383						
KO	M9	0.4% glucose	15.09.2013	0,05	16.09.2013	0,232	17.09.2013	0,391	18.09.2013	0,375	19.09.2013	0,382						
WT	M9	200 µM Lysine	15.09.2013	0,05	16.09.2013	0,052	17.09.2013	0,05	18.09.2013	0,053	19.09.2013	0,043	21.09.2013	0,071	24.09.2013	0,065	25.09.2013	0,074	07.10.2013	0,122
KO	M9	200 µM Lysine	15.09.2013	0,05	16.09.2013	0,051	17.09.2013	0,048	18.09.2013	0,05	19.09.2013	0,043	21.09.2013	0,068	24.09.2013	0,067	25.09.2013	0,066	07.10.2013	0,124
WT	M9	200/400µM K/L	21.09.2013	0,05	24.09.2013	0,036	25.09.2013	0,036	30.09.2013	0,061	07.10.2013	0,133								
KO	M9	200/400µM K/L	21.09.2013	0,05	24.09.2013	0,035	25.09.2013	0,034	30.09.2013	0,065	07.10.2013	0,131								
WT	M9	200/400µM K/L+glucose	21.09.2013	0,05	24.09.2013	0,105	25.09.2013	0,179	30.09.2013	0,185	02.10.2013	0,203	07.10.2013	0,245						
KO	M9	200/400µM K/L+glucose	21.09.2013	0,05	24.09.2013	0,103	25.09.2013	0,185	30.09.2013	0,19	02.10.2013	0,208	07.10.2013	0,232						
WT	M9	.4%glucose H2O2 stress	05.12.2013	0,309	06.12.2013	0,635	06.12.2013	0,754	08.12.2013	1,176	10.12.2013	0,862	12.12.2013	0,752	13.12.2013	0,732				
KO	M9	.4%glucose H2O2 stress	05.12.2013	0,324	06.12.2013	0,695	06.12.2013	0,815	08.12.2013	1,218	10.12.2013	0,943	12.12.2013	0,774	13.12.2013	0,759				
WT	M9	1 mM Lys	05.12.2013	0,103	06.12.2013	0,104	08.12.2013	0,108	10.12.2013	0,116	12.12.2013	0,123	13.12.2013	0,134	15.12.2013	0,18				
KO	M9	1 mM Lys	05.12.2013	0,104	06.12.2013	0,104	08.12.2013	0,107	10.12.2013	0,113	12.12.2013	0,121	13.12.2013	0,128	15.12.2013	0,167				
WT	M9	1 mM Leu	05.12.2013	0,091	06.12.2013	0,089	08.12.2013	0,085	10.12.2013	0,088	12.12.2013	0,086	13.12.2013	0,085						
KO	M9	1 mM Leu	05.12.2013	0,107	06.12.2013	0,099	08.12.2013	0,095	10.12.2013	0,096	12.12.2013	0,093	13.12.2013	0,098						
WT	M9	500 µM Octonoate	05.12.2013	0,113	06.12.2013	0,098	08.12.2013	0,096	10.12.2013	0,099	12.12.2013	0,097	13.12.2013	0,1						
KO	M9	500 µM Octonoate	05.12.2013	0,108	06.12.2013	0,09	08.12.2013	0,089	10.12.2013	0,093	12.12.2013	0,092	13.12.2013	0,091						
WT	M9	10 mM Betaine	06.12.2013	0,081	08.12.2013	0,277	10.12.2013	0,431	12.12.2013	0,369	13.12.2013	0,362	15.12.2013	0,363						
KO	M9	10 mM Betaine	06.12.2013	0,07	08.12.2013	0,256	10.12.2013	0,406	12.12.2013	0,345	13.12.2013	0,335	15.12.2013	0,342						
WT	M9	10 mM Choline	06.12.2013	0,08	08.12.2013	0,088	10.12.2013	0,103	12.12.2013	0,247	13.12.2013	0,352	15.12.2013	0,481	16.12.2013	0,498	17.12.2013	0,512	18.12.2013	0,491
KO	M9	10 mM Choline	06.12.2013	0,067	08.12.2013	0,078	10.12.2013	0,093	12.12.2013	0,211	13.12.2013	0,315	15.12.2013	0,463	16.12.2013	0,483	17.12.2013	0,5	18.12.2013	0,491
WT	M9	10mM Choline + 0,5M NaCl	06.12.2013	0,094	08.12.2013	0,093	10.12.2013	0,065	12.12.2013	0,069	13.12.2013	0,104	15.12.2013	0,305	16.12.2013	0,387	17.12.2013	0,429	18.12.2013	0,482
KO	M9	10mM Choline + 0,5M NaCl	06.12.2013	0,075	08.12.2013	0,087	10.12.2013	0,056	12.12.2013	0,06	13.12.2013	0,078	15.12.2013	0,223	16.12.2013	0,298	17.12.2013	0,393	18.12.2013	0,516
WT	M9	10mM Chol.+.5M NaCl (pregrown chol.)	15.12.2013	0,058	16.12.2013	0,207	17.12.2013	0,286	18.12.2013	0,343										
KO	M9	10mM Chol.+.5M NaCl (pregrown chol.)	15.12.2013	0,057	16.12.2013	0,218	17.12.2013	0,306	18.12.2013	0,385										
WT	M9	10mM Chol.+.6M NaCl (pregrown chol.)	15.12.2013	0,065	16.12.2013	0,141	17.12.2013	0,199	18.12.2013	0,255										
KO	M9	10mM Chol.+.6M NaCl (pregrown chol.)	15.12.2013	0,064	16.12.2013	0,134	17.12.2013	0,198	18.12.2013	0,271										
WT	M9	10 mM Choline (pregrown on YEB)	09.01.2014	0,095	13.01.2014	0,257	15.01.2014	0,615	17.01.2014	0,628	21.01.2014	0,578								
KO	M9	10 mM Choline (pregrown on YEB)	09.01.2014	0,1	13.01.2014	0,259	15.01.2014	0,628	17.01.2014	0,634	21.01.2014	0,583								
WT	M9	10mM Chol.+.3M NaCl (pregrown YEB)	09.01.2014	0,105	13.01.2014	0,071	15.01.2014	0,154	17.01.2014	0,338	21.01.2014	0,544								
KO	M9	10mM Chol.+.3M NaCl (pregrown YEB)	09.01.2014	0,113	13.01.2014	0,08	15.01.2014	0,122	17.01.2014	0,233	21.01.2014	0,584								
WT	M9	10mM Chol.+.5M NaCl (pregrown YEB)	09.01.2014	0,116	13.01.2014	0,061	15.01.2014	0,072	17.01.2014	0,116	21.01.2014	0,506								
KO	M9	10mM Chol.+.5M NaCl (pregrown YEB)	09.01.2014	0,11	13.01.2014	0,056	15.01.2014	0,064	17.01.2014	0,076	21.01.2014	0,397								
WT	M9	10mM Chol.+.7M NaCl (pregrown YEB)	09.01.2014	0,116	13.01.2014	0,058	15.01.2014	0,066	17.01.2014	0,069	21.01.2014	0,095								
KO	M9	10mM Chol.+.7M NaCl (pregrown YEB)	09.01.2014	0,118	13.01.2014	0,061	15.01.2014	0,064	17.01.2014	0,069	21.01.2014	0,086								
WT	M9	10mM Chol.+.3M NaCl (pregrown chol.)	10.01.2014	0,092	13.01.2014	0,127	15.01.2014	0,194	17.01.2014	0,242	21.01.2014	0,284								
KO	M9	10mM Chol.+.3M NaCl (pregrown chol.)	10.01.2014	0,094	13.01.2014	0,104	15.01.2014	0,135	17.01.2014	0,173	21.01.2014	0,255								
WT	M9	10mM Chol.+.5M NaCl (pregrown chol.)	10.01.2014	0,103	13.01.2014	0,085	15.01.2014	0,094	17.01.2014	0,106	21.01.2014	0,168								
KO	M9	10mM Chol.+.5M NaCl (pregrown chol.)	10.01.2014	0,102	13.01.2014	0,076	15.01.2014	0,075	17.01.2014	0,082	21.01.2014	0,183								
WT	M9	10mM Chol.+.7M NaCl (pregrown chol.)	10.01.2014	0,107	13.01.2014	0,075	15.01.2014	0,065	17.01.2014	0,06	21.01.2014	0,076								
KO	M9	10mM Chol.+.7M NaCl (pregrown chol.)	10.01.2014	0,111	13.01.2014	0,08	15.01.2014	0,073	17.01.2014	0,069	21.01.2014	0,075								
WT	M9	0.4% glucose (4.3.2014)	10:00	0,081	11:00	0,083	13:00	0,112	15:00	0,164	17:00	0,264	21:00	0,768	22:00	0,923				
KO	M9	0.4% glucose (4.3.2014)	10:00	0,092	11:00	0,095	13:00	0,117	15:00	0,154	17:00	0,229	21:00	0,627	22:00	0,765				

WT	YEB	(4.3.2014)	10:00 0,134	11:00 0,2	12:00 0,271	13:00 0,38	14:00 0,501	15:00 0,673	16:00 0,883	17:00 1,212	21:00 2,864	22:00 3,151
KO	YEB	(4.3.2014)	10:00 0,124	11:00 0,169	12:00 0,212	13:00 0,273	14:00 0,338	15:00 0,425	16:00 0,538	17:00 0,724	21:00 1,891	22:00 2,151
WT	YEB	15 µM H2O2 (4.3.2014)	10:00 0,141	11:00 0,213	12:00 0,286	13:00 0,389	14:00 0,499	15:00 0,648	16:00 0,808	17:00 1,013	21:00 1,544	22:00 1,745
KO	YEB	15 µM H2O2 (4.3.2014)	10:00 0,127	11:00 0,172	12:00 0,215	13:00 0,275	14:00 0,337	15:00 0,424	16:00 0,533	17:00 0,685	21:00 1,415	22:00 1,646
WT	YEB	15 min of 2 mM H2O2 (4.3.2014)	10:00 0,092	11:00 0,103	12:00 0,112	13:00 0,131	14:00 0,152	15:00 0,177	16:00 0,21	17:00 0,262	21:00 0,64	22:00 0,767
KO	YEB	15 min of 2 mM H2O2 (4.3.2014)	10:00 0,096	11:00 0,103	12:00 0,111	13:00 0,122	14:00 0,134	15:00 0,149	16:00 0,17	17:00 0,204	21:00 0,488	22:00 0,59
WT	M9	10 mM Choline (13.3.2014)	13.03.2014 0,129	14.03.2014 0,113	15.03.2014 0,11	17.03.2014 0,121	18.03.2014 0,196	19.03.2014 0,838	20.03.2014 0,81	21.03.2014 0,781		
KO	M9	10 mM Choline (13.3.2014)	13.03.2014 0,125	14.03.2014 0,11	15.03.2014 0,109	17.03.2014 0,121	18.03.2014 0,153	19.03.2014 0,379	20.03.2014 0,682	21.03.2014 0,818		
WT	M9	10 mM Choline + 0,3M NaCl (13.3.2104)	13.03.2014 0,121	14.03.2014 0,096	15.03.2014 0,091	17.03.2014 0,08	19.03.2014 0,079	20.03.2014 0,081	21.03.2014 0,117			
KO	M9	10 mM Choline + 0,3M NaCl (13.3.2104)	13.03.2014 0,131	14.03.2014 0,11	15.03.2014 0,101	17.03.2014 0,095	19.03.2014 0,094	20.03.2014 0,092	21.03.2014 0,102			
WT	M9	10 mM Choline + 0,4M NaCl (13.3.2014)	13.03.2014 0,138	14.03.2014 0,109	15.03.2014 0,1	17.03.2014 0,083						
KO	M9	10 mM Choline + 0,4M NaCl (13.3.2014)	13.03.2014 0,128	14.03.2014 0,101	15.03.2014 0,094	17.03.2014 0,079						
WT	M9	10 mM Betaine (13.3.2014)	13.03.2014 0,136	14.03.2014 0,181	15.03.2014 0,626	17.03.2014 0,684	18.03.2014 0,682					
KO	M9	10 mM Betaine (13.3.2014)	13.03.2014 0,13	14.03.2014 0,187	15.03.2014 0,695	17.03.2014 0,684	18.03.2014 0,673					
WT	M9	10 mM Betaine + 0,3M NaCl (13.3.2014)	13.03.2014 0,131	14.03.2014 0,104	15.03.2014 0,1	17.03.2014 0,116	18.03.2014 0,178	19.03.2014 0,372	20.03.2014 0,5	21.03.2014 0,693		
KO	M9	10 mM Betaine + 0,3M NaCl (13.3.2014)	13.03.2014 0,14	14.03.2014 0,114	15.03.2014 0,106	17.03.2014 0,114	18.03.2014 0,133	19.03.2014 0,234	20.03.2014 0,337	21.03.2014 0,585		
WT	M9	10 mM Betaine + 0,4M NaCl (13.3.2014)	13.03.2014 0,131	14.03.2014 0,106	15.03.2014 0,095	17.03.2014 0,083	18.03.2014 0,077	19.03.2014 0,079	20.03.2014 0,081	21.03.2014 0,104		
KO	M9	10 mM Betaine + 0,4M NaCl (13.3.2014)	13.03.2014 0,134	14.03.2014 0,109	15.03.2014 0,097	17.03.2014 0,081	18.03.2014 0,079	19.03.2014 0,085	20.03.2014 0,088	21.03.2014 0,118		
WT	M9	10 mM Sarcosine (13.3.2014)	13.03.2014 0,127	14.03.2014 0,124	15.03.2014 0,155	17.03.2014 0,498	18.03.2014 0,591	19.03.2014 0,548	20.03.2014 0,53			
KO	M9	10 mM Sarcosine (13.3.2014)	13.03.2014 0,122	14.03.2014 0,126	15.03.2014 0,158	17.03.2014 0,532	18.03.2014 0,57	19.03.2014 0,529	20.03.2014 0,52			
WT	M9	10 mM Sarcosine + .3M NaCl (13.3.2014)	13.03.2014 0,121	14.03.2014 0,111	15.03.2014 0,106	17.03.2014 0,129	18.03.2014 0,159	19.03.2014 0,239	20.03.2014 0,31	21.03.2014 0,489		
KO	M9	10 mM Sarcosine + .3M NaCl (13.3.2014)	13.03.2014 0,126	14.03.2014 0,116	15.03.2014 0,113	17.03.2014 0,145	18.03.2014 0,178	19.03.2014 0,262	20.03.2014 0,332	21.03.2014 0,505		
WT	M9	10 mM Sarcosine + .4M NaCl (13.3.2014)	13.03.2014 0,119	14.03.2014 0,103	15.03.2014 0,096	17.03.2014 0,1	18.03.2014 0,106	19.03.2014 0,127	20.03.2014 0,141	21.03.2014 0,184		
KO	M9	10 mM Sarcosine + .4M NaCl (13.3.2014)	13.03.2014 0,123	14.03.2014 0,106	15.03.2014 0,101	17.03.2014 0,106	18.03.2014 0,113	19.03.2014 0,134	20.03.2014 0,147	21.03.2014 0,189		
WT	M9	10mM Chol. (pregrown chol.) 3.4.2014	Start 0,062	2h 0,07	4h 0,085	5h 0,096	23h 0,634	24h 0,654	25h 0,684	26h 0,714	28h 0,829	30h 0,828
KO	M9	10mM Chol. (pregrown chol.) 3.4.2014	Start 0,04	2h 0,04	4h 0,066	5h 0,078	23h 0,412	24h 0,439	25h 0,474	26h 0,505	28h 0,564	30h 0,61
WT	M9	10mM Chol.+.3M NaCl(pregrown chol.)	Start 0,039	5h 0,055	23h 0,194	25h 0,221	27h 0,257	29h 0,296	30h 0,316	49h 0,789	50h 0,798	
KO	M9	10mM Chol.+.3M NaCl(pregrown chol.)	Start 0,034	5h 0,046	23h 0,136	25h 0,15	27h 0,168	29h 0,187	30h 0,196	49h 0,523	50h 0,541	
WT	M9	10mM Beta. (pregrown beta.) 3.4.2014	Start 0,022	2h 0,033	4h 0,052	5h 0,063	23h 0,418	24h 0,449	25h 0,481	26h 0,512	28h 0,573	30h 0,652
KO	M9	10mM Beta. (pregrown beta.) 3.4.2014	Start 0,023	2h 0,022	4h 0,031	5h 0,043	23h 0,483	24h 0,521	25h 0,557	26h 0,594	28h 0,657	30h 0,654
WT	M9	10mM Beta.+.3M NaCl (pregrown beta.)	Start 0,016	5h 0,022	23h 0,107	25h 0,115	27h 0,128	29h 0,14	30h 0,148	49h 0,356	50h 0,366	
KO	M9	10mM Beta.+.3M NaCl (pregrown beta.)	Start 0,037	5h 0,025	23h 0,134	25h 0,148	27h 0,164	29h 0,183	30h 0,196	49h 0,466	50h 0,479	
WT	M9	10 mM Sarcosine (pregrown sarcosine)	Start 0,008	2h 0,05	4h 0,058	5h 0,06	23h 0,095	49h 0,176	73h 0,179	149h 0,14		
KO	M9	10 mM Sarcosine (pregrown sarcosine)	Start 0,001	2h 0,037	4h 0,044	5h 0,048	23h 0,081	49h 0,16	73h 0,172	149h 0,139		
WT	M9	10mM Sarc.+.3M NaCl (pregrown sarc.)	Start 0,023	5h 0,018	23h 0,017	49h 0,015	73h 0,07	149h 0,236				
KO	M9	10mM Sarc.+.3M NaCl (pregrown sarc.)	Start 0,038	5h 0,037	23h 0,035	49h 0,034	73h 0,134	149h 0,216				